Astron. Astrophys. 354, 169–187 (2000)

ASTRONOMY AND ASTROPHYSICS

Mixing along the red giant branch in metal-poor field stars⋆,⋆⋆

R.G. Gratton[1], **C. Sneden**[2], **E. Carretta**[1], **and A. Bragaglia**[3]

[1] Osservatorio Astronomico di Padova, Vicolo dell'Osservatorio 5, 35142 Padova, Italy (gratton@pd.astro.it)
[2] Department of Astronomy and McDonald Observatory, The University of Texas at Austin, USA (chris@verdi.as.utexas.edu)
[3] Osservatorio Astronomico di Bologna, Italy

Received 26 August 1999 / Accepted 19 November 1999

Abstract. We have determined Li, C, N, O, Na, and Fe abundances, and ^{12}C/^{13}C isotopic ratios for a sample of 62 field metal-poor stars in the metallicity range $-2 \leq$[Fe/H]≤ -1. Stars were selected in order to have accurate luminosity estimates from the literature, so that evolutionary phases could be clearly determined for each star. We further enlarged this dataset by adding 43 more stars having accurate abundances for some of these elements and similarly well defined luminosities from the literature. This large sample was used to show that (small mass) lower-RGB stars (i.e. stars brighter than the first dredge-up luminosity and fainter than that of the RGB bump) have abundances of light elements in agreement with predictions from classical evolutionary models: only marginal changes occur for CNO elements, while dilution within the convective envelope causes the surface Li abundance to decrease by a factor of ~ 20. A second, distinct mixing episode occurs in most (perhaps all) small mass metal-poor stars just after the RGB bump, when the molecular weight barrier left by the maximum inward penetration of the convective shell is canceled by the outward expansion of the H-burning shell, in agreement with recent theoretical predictions. In field stars, this second mixing episode only reaches regions of incomplete CNO burning: it causes a depletion of the surface ^{12}C abundance by about a factor of 2.5, and a corresponding increase in the N abundance by about a factor of 4. The ^{12}C/^{13}C is lowered to about 6 to 10 (close to but distinctly higher than the equilibrium value of 3.5), while practically all remaining Li is burnt. However an O-Na anti-correlation such as typically observed amongst globular cluster stars, is not present in field stars. None of the 29 field stars more evolved than the RGB bump (including 8 RHB stars) shows any sign of an O depletion or Na enhancement. This means that the second mixing episode is not deep enough to reach regions were ON-burning occurs in field stars.

Key words: stars: Hertzsprung–Russel (HR) and C-M diagrams – stars: evolution – stars: Population II – Galaxy: globular clusters: general

Send offprint requests to: R.G. Gratton

⋆ Based in part on observations made at the ESO La Silla Observatory

⋆⋆ Tables 1, 2, 3, 5 and 6 are available in electronic form only at the CDS via anonymous ftp to cdsarc.u-strasbg.fr(130.79.128.5) or via http://cdsweb.u-strasbg.fr/Abstract.html

1. Introduction

Stellar models predict that as a small mass star evolves up the red giant branch (RGB), the outer convective envelope expands inward and penetrates into the CN-cycled processed interior regions. The ensuing mixing episode, called the "first dredge-up" is predicted (Iben 1964) to alter the star's surface light element abundances. For example, in theoretical solar mass/metallicity stars a moderate depletion of ^{12}C (by factor of ~ 2) occurs, lowering the ^{12}C/^{13}C ratio from the original value (assumed to be nearly solar) down to about 20–30, and increasing the ^{14}N content by a corresponding amount (Iben & Renzini 1984). The expansion of the convective envelope also causes a dilution of the Li preserved in the outer stellar surface regions, so that the Li abundance decreases by a factor of about 20 from the original value observed in main sequence stars. First dredge up is expected to be less efficient in metal-poor stars (VandenBerg & Smith 1988; Charbonnel 1994): for a stellar model with metal content $Z = 0.001$ and a mass of 0.8 $M_{\odot}$, changes in C and N abundances are very small, and the ^{12}C/^{13}C ratio is expected to remain > 30.

Results for old disk field giants (Cottrell & Sneden 1986; Shetrone et al. 1993) and metal-poor stars (Sneden et al. 1986) show that the first dredge-up occurs at approximately the predicted luminosities; however, mixing in old, metal-poor, small-mass bright giants is much more extreme than predicted by evolutionary models. These stars have values of the ^{12}C/^{13}C ratio lower than 10 (Lambert & Sneden 1977; Sneden et al. 1986), and no detectable Li at all (Sneden et al. 1986; Pilachowski et al. 1993). However, due to the poor knowledge of the intrinsic luminosities (and hence evolutionary status), it is not easy to understand if this abundance pattern is due to deeper mixing at first dredge-up, or to some other mixing episode.

Recent theoretical studies (e.g. Charbonnel 1994, 1995), extending pioneering work by Sweigart & Mengel (1979), have demonstrated that some further mixing is likely possible in the advanced phases of the RGB: in fact, after the end of the dredge-up phase is reached, the convective envelope begins to recede, leaving behind a chemical discontinuity; the corresponding change in molecular weight prevents further mixing (the so-called $\mu-$barrier). However, during evolution along the RGB this discontinuity is subsequently contacted by the outward ad-

vancing H-burning shell and when this occurs the $\mu-$barrier is effectively canceled out. The immediate effect is to feed fresh hydrogen fuel into the burning shell, causing a temporary stoppage (slowdown) in the star's evolution along the RGB. This slowdown can be clearly seen as a pile up of stars at this (L, $T_{\rm eff}$) position, which thereby is called the RGB "LF bump". The RGB bump may be clearly seen in colour-magnitude diagrams of globular clusters (King et al. 1985; Zoccali et al. 1999) at the luminosities predicted by most recent models (see e.g. Cassisi et al. 1997), that is slightly larger than the horizontal branch for metal-poor stars ([Fe/H]< -1). Thereafter, since there is no molecular weight gradient between the convective envelope and the near vicinity of the shell, it is possible that circulation currents (perhaps driven by meridional circulations activated by core rotation, Sweigart & Mengel 1979) could give rise to a further mixing episode. We will hereafter define as lower red giant branch (lower-RGB) the evolutionary phase between first dredge-up completion and the RGB bump: according to the above sketched scenario, small mass stars on the lower-RGB should have a well defined set of CNO and Li abundances, distinct from that observed in main sequence stars (MS stars, which have not yet experienced the first dredge up) and upper-RGB stars (hereinafter, upper-RGB stars are those stars first ascending the red giant branch, which are brighter than the RGB bump).

In principle, globular clusters offer a unique opportunity to verify this scheme, since they provide a large number of stars located at a similar distance (allowing an accurate definition of the evolutionary status of individual stars), having the same age (thus similar masses evolving along the RGB), and hopefully the same initial chemical composition. As a matter of fact, much of our knowledge about stellar evolution is drawn from cluster observations. A large number of authors have tried to exploit this opportunity, and in fact promising hints for a mixing episode occurring at or after the RGB-bump have been found in early studies of the most metal-poor clusters M92 (Carbon et al. 1982), M15 (Trefzger et al. 1983), and NGC 6397 (Briley et al. 1990). However, surface abundances of globular cluster RGB stars have revealed a complex phenomenology (for a summary, see Kraft 1994), that has so far defied insofar any attempt of a detailed explanation. This is likely due to the fact that the surface abundances of these stars are significantly affected by several major factors: deep mixing within individual stars, primordial inhomogeneities within a cluster, and perhaps accretion of nuclearly processed material during the early phases of the cluster evolution. Furthermore, it is becoming increasingly clear that the dense environment plays an important role on determining other basic cluster features (like the colour of the horizontal branch), either by causing systematic variations in the basic stellar properties (like the initial angular momentum), or in favouring pollution of the surface layers of stars by ejecta from other stars, or both.

To solve these issues, it is necessary to first understand the evolution of single undisturbed small mass stars (very wide binaries may be considered here as single stars): this is now possible thanks to the parallax data from the Hipparcos satellite, and to the efforts of a number of investigators who determined accurate physical parameters (temperatures and luminosities) for large samples of metal-poor giants, disentangling the effects of reddening, metal abundance, and binarity (see e.g. Schuster & Nissen 1989; Carney et al. 1994; and Anthony-Twarog & Twarog 1994).

In this paper we report new abundances of Li, C, N, O, Na, and ^{12}C/^{13}C ratios for a large sample of metal-poor ($-2 <$[Fe/H]< -1) stars for which the evolutionary phases could be accurately ascertained. The sample was selected in order to include field stars in a restricted range in mass (observed stars belong to the halo and the thick disk) and metal abundance, to avoid problems in data interpretation due to fact that luminosity of the first dredge-up and of the RGB bump indeed depends on both metallicity and mass. To this purpose we exploited luminosities derived from Hipparcos parallaxes, as well as those that can be inferred from Strömgren photometry (see Anthony-Twarog & Twarog 1994). To give more significance to our results, whenever possible we complemented our original analysis with data gathered from the literature, either by reanalyzing original EWs, or, when this was not possible, by applying systematic corrections to reduce original abundances to the system used throughout this paper.

In Sect. 2 we describe our original sample. In Sect. 3 details about the observations and reductions are given. Derivation of the atmospheric parameters for the programme stars is discussed in Sect. 4. In Sect. 5 we explain the procedures used to derive abundances from atomic and molecular lines. In Sect. 6 we compare our results with literature values, and compile an extended table of abundances for metal-poor stars, mainly in the metallicity bin of interest in this paper. In Sect. 7 we use these data to discuss mixing episodes along the RGB, and summarize our conclusions in Sect. 8.

2. Sample selection

The original sample consisted of stars with $-2 <$[Fe/H]< -1 from the papers by Anthony-Twarog & Twarog (1994: hereinafter ATT) for evolved stars, and Schuster & Nissen (1989) for main sequence and turn-off stars. Note that our defined metallicity limits refer to the original values listed by ATT and Schuster & Nissen: these sometimes were different from those determined in our analysis, so that a few observed stars scattered out of the original metallicity bin. The abundance range was selected in order to have a sample cleaned of possible massive interlopers (thin disk stars), with a large enough number of relatively bright stars having accurately determined absolute magnitudes (in order to clearly mark the evolutionary phase for each star), and avoiding complications related to large star-to-star abundance variations present amongst the most metal-poor stars (McWilliam et al. 1995). While we did not derive galactic velocity components for all stars in our sample (although this would be possible using Hipparcos data), data available from the literature (Carney et al. 1994; Hanson et al. 1998) show that the programme stars are a mix of mostly halo and a few metal-poor thick disk stars. Various authors (see in particular

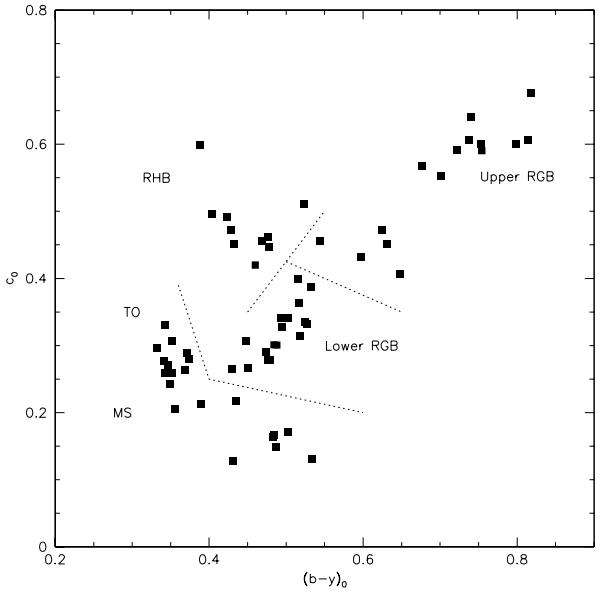

Fig. 1. $(b-y)_0 - c_0$ diagram for the programme stars. Different evolutionary phases as defined in this paper are marked. Lower-RGB and upper-RGB stars are stars climbing-up the RGB below and above the RGB bump respectively

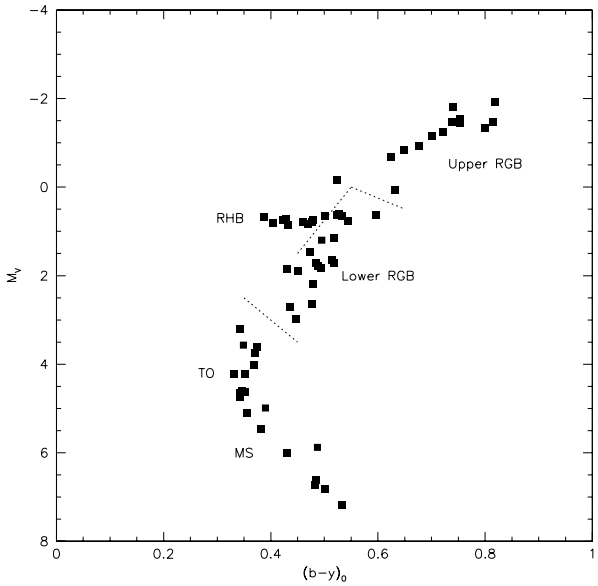

Fig. 2. Colour-magnitude diagram for the programme stars. Different evolutionary phases as defined in this paper are marked. lower-RGB and upper-RGB stars are stars climbing-up the RGB below and above the RGB bump respectively

Gratton et al. 1996, Nissen & Schuster 1997, and Fuhrmann 1998) have shown that most halo and thick disk dwarfs have similar element-to-element abundance ratios (in particular, the same overabundances of O and $\alpha-$elements), and that the spread in the element-to-element abundance ratios is generally small (see e.g. Gratton & Sneden 1991), in the abundance range considered in this paper (-2 <[Fe/H]< -1), although both these assertions are not true outside of this range. As a matter of fact, even within the range -2 <[Fe/H]< -1 there are a few halo dwarfs known to have clearly anomalous abundances (some of them being in our sample, such as HD25329 and HD134439), and more tiny star-to-star differences can be shown to exist by careful differential comparisons of stars with very similar atmospheric parameters (see e.g. Jehin et al. 1999). However, these last differences are generally so small that we may assume that most of the stars in our sample formed with approximately the same mixture of heavy elements (within ~ 0.1 dex); we will discuss separately the few stars with clearly anomalous abundances.

Our sample was constrained to have about ten-fifteen stars in each of the following evolutionary phases:

- MS and turn off (TO) stars (primordial CNO abundances)
- lower-RGB stars (first dredge-up)
- upper-RGB stars (further mixing mechanism)
- Red horizontal branch (RHB stars, post He-flash)

Membership of stars in these evolutionary phases was determined from their position on the $(b-y)_0 - c_0$ diagram (Fig. 1); however, it is well confirmed by their position in the colour-magnitude diagram (Fig. 2). We added to this sample a few local subdwarfs, whose spectra were taken for another programme (Clementini et al. 1998).

The total sample consists of 62 stars. Basic data for the programme stars are given in Table 1 (only available in electronic form). We listed V magnitudes, $B-V$ and $b-y$ colours and m_1 and c_1 indices. Whenever possible, reddening for the giants were from ATT; these were in turn derived from the reddening maps of Burstein & Heiles (1982), taking into account stellar distances using a modified cosecant-law; they should have errors of ~ 0.03 mag in $E(B-V)$ and ~ 0.02 mag in $E(b-y)$. We assumed that dwarfs are unreddened: this is reasonable in view of their small distances. The last three columns provide the absolute visual magnitude M_V derived from Hipparcos parallaxes and those listed by ATT, as well as our finally adopted value. These were from ATT whenever possible (i.e. for giants and subgiants); else they were derived from the Hipparcos parallaxes (highly reliable for dwarfs, but quite inaccurate for the intrinsically brightest stars). A cross check between the two sets (see Fig. 3) shows a good agreement between the two scales in the region of overlap; a similar result has been obtained also by Hanson et al. (1998).

3. Observations

High S/N (> 100), high resolution ($R > 50,000$) spectra of the programme stars were obtained using the McDonald 2.7 m telescope and the ESO CES telescope. Data were acquired for each star to analyze the following spectral features:

- the O I IR triplet (at 7771-74 Å) and the [OI] line (at 6300 Å)
- sections of the $A^2\Pi - X^2\Delta$ CH G-band (near 4235 and 4365 Å), which allows determination of both the abundance of ^{12}C and of the ^{12}C/^{13}C ratio
- the Na I doublets at 6154-60 Å and 5682-88 Å
- the Li I 6707 Å resonance doublets

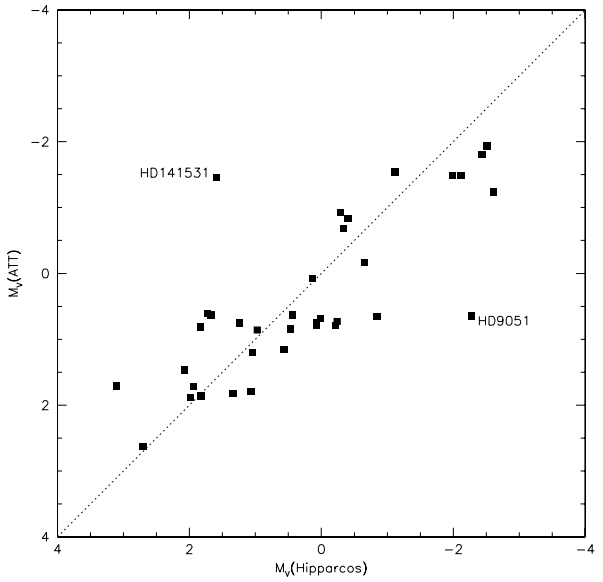

Fig. 3. Comparison between absolute magnitudes from Hipparcos parallaxes and those by ATT

– a number of Fe I and Fe II lines scattered throughout the same wavelength ranges
– although this was not in the original baseline of our observations, the wide spectral coverage of the McDonald spectra also allowed observation of the $B^2\Sigma - X^2\Sigma\ \Delta v = 0$ CN bandhead near 3880 Å; coupled with the C abundances from the G-band, these observations gave N useful abundances for about a third of the sample

The very broad spectral coverage of our McDonald spectra allowed us to measure a large number of additional spectral features not relevant to this study. This material will be used in a future paper for a better discussion of the abundances of a number of elements in this metal abundance range. Here, we exploit the large number of Fe I and Fe II lines measured for an accurate determination of the Fe abundance and of the microturbulent velocity.

The ESO CAT telescope was used to gather spectra of southern stars with the CES spectrograph in two runs during 1995. In the May run, we used the Short Camera with a 1024×640 high resolution RCA CCD (ESO #9, pixel size 15 μm); this configuration was not available for the November run, so that instead we used the Long Camera and a Loral CCD detector (ESO #38) with 2,670 pixels along the dispersion (pixel size 15 μm). Both configurations allowed similar spectral coverage ($\sim\ \lambda/120$), the larger size of the Loral CCD compensating the longer focal length of the camera. Spectral regions centered at 4230, 4380, 5680, 6300, 6700, and 7780 Å were acquired in both cases. Resolving power $R = \lambda/\Delta\lambda$ was set at 50,000 by adjusting the slit width: this resulted in some oversampling for the Long Camera observations (in that case ~ 5 pixels covered a resolution element along dispersion). The signal-to-noise S/N ratio of the spectra was greater than ~ 150, save for the bluest spectra which have lower S/N (~ 80 in the worst cases).

The McDonald data were obtained with the "2d-coudé" echelle spectrometer (Tull et al. 1995). The spectrograph was configured to have spectral range 3800$\leq \lambda \leq$9000 Å (continuous wavelength coverage for echelle orders with $\lambda < 5800$ Å, and gaps redward of this due to ever-increasing length of the orders). The spectrograph entrance aperture of 1.2 arcsec projected to a 2-pixel measured resolving power of $R \simeq 60,000$ at the TeK 2048×2048 CCD detector. Signal-to-noise ratios of the spectra were lowest in the blue orders, due to lower CCD quantum efficiencies and lower fluxes from our cool stars at these wavelengths, but always exceeded $S/N \simeq 100$ at 4200 Å and $S/N \simeq 70$ at 3880 Å.

For both ESO and McDonald observations, spectra of fast rotating early-type stars were also acquired: they were used to remove contamination due to the telluric features.

Spectra were reduced as usual by means of routines within IRAF: this included bias and background subtraction, flat field division, cosmic ray excision, order extraction, wavelength calibration, and division for the spectrum of a rapidly rotating early type star spectrum for those orders where telluric contamination was expected to be important (mainly the region of the [OI] line)

3.1. Equivalent widths

Equivalent widths for a large number of lines of various elements were measured by means of a Gaussian fitting routine within the ISA package software (Gratton 1988); those for O and Na lines are given in Table 2 (only available in electronic form). Since damping wings are neglected by this procedure, equivalent widths are systematically underestimated for the strongest lines. To avoid systematic errors on the microturbulent velocities, we only considered Fe lines with equivalent widths EWs smaller than

$$\log \frac{EW}{\lambda} < -4.5 - 0.1 \log g. \quad (1)$$

We compared our EW's with those measured by other authors. An extensive comparison is possible for the McDonald spectra. The agreement is generally good. Mean differences (in the sense this paper – previous authors) and residuals with other authors are as follows:

– Zhao & Magain (1990): -1.7 ± 1.2 mÅ ($\sigma = 6.2$ mÅ, 29 lines)
– Edvardsson et al. (1993): -1.1 ± 0.8 mÅ ($\sigma = 3.1$ mÅ, 16 lines)
– Tomkin et al (1992) and Sneden et al. (1991): $+0.7 \pm 0.6$ mÅ ($\sigma = 5.3$ mÅ, 78 lines)

Here σ is the r.m.s. scatter for individual values.

A comparison of EWs measured on the CAT spectra with those measured on the McDonald spectra and with literature values shows that these EWs are systematically too large. They were corrected according to the following formulas:

$$EW_{\rm corr} = 0.915\ EW_{\rm meas} - 4.2 \text{ if } EW > 15.5 \text{ mÅ} \quad (2)$$

$$EW_{\rm corr} = 0.644\ EW_{\rm meas} \text{ if } EW < 15.5 \text{ mÅ} \quad (3)$$

Typical errors in the CAT EW's are about ± 5 mÅ

Whenever possible, we complemented the CAT EWs with lists of accurate EWs (typical errors < 3 mÅ) from the literature (Gratton 1989, Zhao & Magain 1990, Sneden et al. 1991, Spite & Spite 1991, Tomkin et al. 1992, Edvardsson et al. 1993, Beveridge & Sneden 1994, Carretta et al. 1999). These complementary data were available for 13 stars.

4. Atmospheric parameters

Effective temperatures $T_{\rm eff}$ were derived from dereddened $(B-V)_0$ and $(b-y)_0$ colours using the colour-$T_{\rm eff}$ transformations from Kurucz (1995); use of this uniform approach allows us to compare abundances for stars over a broad range in atmospheric parameters (temperatures and luminosities), and whose spectral data are of quite different extent. Note that models computed for this paper had the convective overshooting option switched off: these models better reproduce observed features in both the Sun and metal-poor stars (Castelli et al. 1997). Temperatures derived from the two colours agree fairly well, the average difference being 24 ± 9 K ($\sigma = 71$ K) in the sense that temperatures from $(B-V)$ colours are higher. For three RHB stars (HD 20, HD 105546, HD 110885) temperatures from the $b-y$ colour are ~ 200 K larger than those from $B-V$; however, the agreement between the two temperatures is good for the remaining RHB stars, so that we decided to simply average temperatures given by the two colours.

Internal uncertainties in these $T_{\rm eff}$'s are due to errors in the colours for individual stars and in the assumed reddening; we estimate they are about ± 50 K for the dwarfs (corresponding to an error of about ± 0.02 mag in $(B-V)_0$, and ± 0.015 mag in $(b-y)_0$), and somewhat larger for giants; however uncertainties may be larger for a few stars with less well determined reddenings.

We may compare our effective temperatures for dwarfs with those determined by Alonso et al. (1996) using the Infrared Flux Method. Most of the weight in this procedure is in the IR colours, so that these $T_{\rm eff}$'s can be effectively considered to be independent from ours. We have 9 stars in common with their sample. On average, temperatures we used are higher than those of Alonso et al. by 54 ± 21 K, with $\sigma = 84$ K for the residuals for individual stars (note that the mean quadratic error given by Alonso et al. for these 9 stars is 75 K, so that this scatter agrees with our estimates for errors in individual $T_{\rm eff}$'s). Other useful comparisons regard giants: among the various choices possible, we decided to compare our $T_{\rm eff}$'s with those adopted by Sneden et al. (1991) and Kraft et al. (1992). $T_{\rm eff}$'s adopted by these authors were derived with the constraint that no trend of abundances from Fe I lines with excitation was obvious in their analysis: again, this procedure is completely independent of ours. Our temperatures are on average higher than those used by these authors by 60 ± 22 K for 8 stars in common ($\sigma = 63$ K). These comparisons suggest that scale errors in our $T_{\rm eff}$'s should not exceed 50-100 K. Since we are mainly interested in differential abundance effects rather than on absolute abundances, and since the effects we want to show are quite large, we regard as minor the uncertainties related to the temperature scale.

Gravities were derived as:

$$\log \frac{g}{g_\odot} = \log \frac{M}{M_\odot} + 0.4(M_V + BC - 4.72) + 4 \log \frac{T_{\rm eff}}{T_\odot} \quad (4)$$

assuming a mass of $M = 0.85$ M$_\odot$ for all stars and BC's from Kurucz (1995).

To estimates uncertainties in our gravities, we proceeded as follows. First we noted that since uncertainties in temperatures, masses and bolometric corrections are small, errors in $\log g$ (and luminosities) are essentially 0.4 times the uncertainty in the absolute magnitudes M_V's. ATT determined the absolute magnitudes for field giants by assuming they are the same as those of cluster stars with the same metallicity and $(b-y)_0$ colour. This comparison could be wrong if there are errors in stellar metallicities and reddenings. Stated uncertainties in ATT metallicities are ± 0.16 dex. Cluster red giant branches become redder with increasing metallicity, with a slope of ~ 0.18 mag/dex for the $(b-y)_0$ colour[1]. The implied uncertainty in the fittings amounts then to 0.029 mag in $(b-y)$. We summed quadratically this value to the uncertainty in reddenings (about 0.02 mag in $E(b-y)$), and obtained a total fitting error of ± 0.035 mag in $(b-y)$. If we now take into account the typical slope of the RGB in the colour-magnitude diagram ($M_V - (b-y)_0$), that is ~ 13, we conclude that typical errors in the absolute magnitudes M_V's are about 0.45 mag. Typical errors in our gravities are then ~ 0.2 dex (with some allowance for errors in $T_{\rm eff}$'s and masses). Errors are lower (~ 0.1 dex) for the subdwarfs, which have good Hipparcos parallaxes (generally, parallax errors are $\leq 10\%$ for dwarfs in our sample). Again, errors may be larger for a few stars, if reddening has been misestimated.

We obtained microturbulent velocities v_t for those stars with McDonald spectra and those stars with more than 15 lines from CAT spectra eliminating trends of abundances derived from Fe I lines of different EW's (see next section for our gf choice). The large number of lines measured in these spectra allowed an accurate determination of this parameter (internal errors are within 0.15 km s^{-1}). The values determined by this procedure correlate very well with the location in the c-m diagram: it was then possible to derive a tight relation between microturbulence velocity, effective temperatures and surface gravity, with $\sigma = 0.16$ km s^{-1} (see Fig. 4). This was used to derive values of the microturbulent velocity for stars with CAT spectra when fewer than 15 Fe lines were measured. For RGB stars with $T_{\rm eff} < 5500$ K, the present relation matches well the values obtained using the formula given by Pilachowski et al. (1996); however, values are quite different for MS and TO stars (stars in these evolutionary phases were not considered by Pilachowski et al.). In agreement with Pilachowski et al., we found that RHB stars have larger microturbulent velocities than RGB stars of

[1] This slope was obtained by combining the relation between $(b-y)$ and $(B-V)$ colours for giants given by ATT, with the metallicity calibration of the $(B-V)_{0,g}$ index for globular clusters given by Gratton & Ortolani (1989)

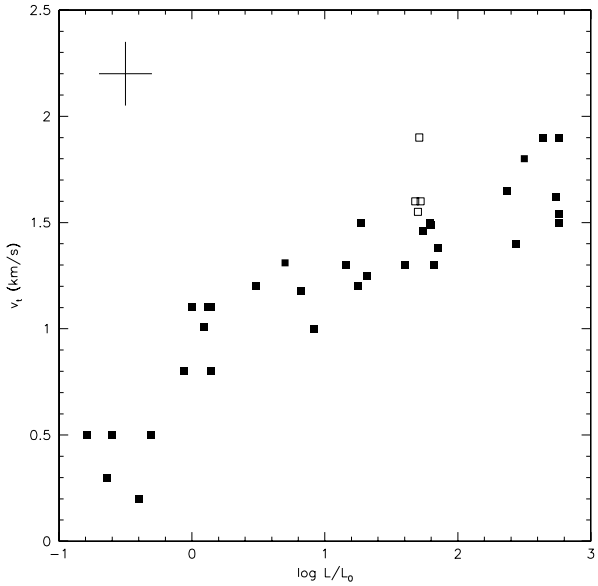

Fig. 4. Run of microturbulent velocities v_t with luminosities for those stars with more than 15 Fe I lines measured (these are the stars for which microturbulent velocities could be determined by eliminating trends of abundances with excitation potential). Filled symbols are MS and first ascent RGB stars; open symbols are RHB stars. Typical error bar is shown at top left

similar temperature and luminosities, with values in the range 1.5-2.0 km s^{-1}.

5. Abundance analysis

Abundances for Fe I, Fe II, O I, and Na I were derived from measured equivalent widths (EW's); those for Li, C, N, and the ^{12}C/^{13}C ratio by comparisons with synthetic spectra. The abundance analysis was performed using Kurucz (1995) model atmospheres with no overshooting. These models are computed with solar-scaled abundances of heavy elements. However, we checked that when they are replaced with models computed with a non-solar scaled mixture (enhanced abundances of O and $\alpha-$elements), unfortunately only available at [Fe/H]=-2 for this test (Castelli 1998, private communication), the net effect on the ratios [element/Fe] is small (≤ 0.02 dex).

Iron abundances from Fe I lines are given in Column 8 of Table 3 (only available in electronic form), along with the number of lines used (Column 7) and the σ of abundances from individual lines (Column 9). The r.m.s. average of this scatter is 0.11 dex; this is approximately what is expected given the quality of the observational material. Our stellar [Fe/H] values were obtained by comparing the abundances we obtained from the analysis of the stellar EW's with those obtained by an analogous analysis of the EW's for the Sun for a line set essentially similar to that used for the programme stars, and using the Kurucz (1995) solar model atmosphere. Fe I gf's were taken from Bard et al. (1991) and Bard & Kock (1994); from the Oxford group experiments (Blackwell et al. 1995 and references therein, corrected upward by 0.03 dex to put them on the scale of Bard et al.), and from an inverse solar analysis using the Fe abundance determined from those lines having laboratory gf's and EW's from Rutten & Van der Zalm (1984). The solar Fe abundance we get (with our choice of gf's) is $\log\epsilon(Fe) = 7.51$, coincident with the meteoritic value (Anders & Grevesse 1989). Note that our [Fe/H]'s are derived from an analysis fully consistent with that for the other elements; they may be a little bit different from other published values, mainly due the adoption of a different $T_{\rm eff}$'s scale. Note also that in our analysis, trends of abundances with excitation potential show some scatter, but no convincing evidence for systematic trends.

Abundances from Fe II lines were also available for the majority of the programme stars; they are given in Column 10 of the same table. These were obtained using gf's from laboratory experiments (lifetimes and branching ratios: Holweger et al. 1990; Biemont et al. 1991b, Hannaford et al. 1992). The solar abundance of Fe obtained with these gf's is $\log\epsilon(Fe) = 7.45$, somewhat lower than estimated from neutral lines. This difference of abundances derived from different species of the same element should not be a surprise, since apart from possible systematic errors in the adopted gf's, it is also well known that the Kurucz (1995) constant flux solar model atmosphere is not a perfect representation of the real solar atmosphere (see e.g. Castelli et al. 1997). However, in the spirit of a strictly differential analysis, stellar abundances for Fe II given in this paper are obtained using our value of Fe II for the Sun, so that uncertainties in the gf's and in the model atmospheres should largely cancel out.

A comparison between Fe abundances derived from neutral and singly ionized lines allows an overall test of the adopted atmospheric parameters, in particular temperatures and gravities, since these last were not derived from the equilibrium of ionization. On average, abundances with respect to the Sun from Fe I and II agree very well, suggesting that the previously mentioned uncertainties in gf's and model atmospheres really canceled out: the mean difference is 0.00 ± 0.02 dex, with $\sigma = 0.11$ dex, based on 40 stars[2]. The scatter agrees well with, and supports our estimates of uncertainties in the adopted atmospheric parameters: in fact given the sensitivities listed in Table 4, we would expect a σ for the difference Fe II-Fe I of 0.15 dex for giants, and 0.09 dex for dwarfs.

Column 11 of Table 3 gives the reference for the EWs: M marks EW's measured on McDonald spectra, C are those from the CAT spectra, while L marks EW's gathered from high S/N (> 150), high resolution ($R \geq 30,000$) data available in the literature. Finally the last column of Table 3 gives the evolutionary phase of the stars as deduced from the $(b-y)_0 - c_0$ diagram (MS are main sequence and TO stars; lower-RGB are RGB stars

[2] There is actually a small trend for slightly larger (~ 0.05 dex) abundances from Fe II lines for giants, and the opposite for dwarfs; this suggests that temperatures are underestimated by ~ 50 K for giants, and overestimated by a similar quantity for dwarfs. These differences might indicate small inadequacies of the adopted model atmospheres, or systematic errors in the adopted reddenings. The impact of such inadequacies on the result of our paper is small, and will be neglected hereinafter

Table 4. Sensitivity of abundances on atmospheric parameters

	$T_{\rm eff}$	$\log g$	[A/H]	v_t	Total
Change	+100 K	+0.2 dex	+0.1 dex	+0.2 km s^{-1}	
			HD 2665		
[Fe/H] I	0.110	-0.013	-0.006	-0.032	0.12
[Fe/H] II	-0.006	0.071	0.009	-0.025	0.08
$\log \epsilon(Li)$	0.117	-0.012	-0.003	0.000	0.12
[C/Fe] CH	0.080	-0.035	0.042	0.019	0.10
[N/Fe] CN	0.190	-0.027	0.066	0.032	0.21
[O/Fe] [OI]	0.072	0.002	0.007	0.025	0.08
[O/Fe] OI	-0.113	0.006	-0.014	0.019	0.12
[Na/Fe]	-0.050	0.005	0.003	0.022	0.06
			HD 194598		
[Fe/H] I	0.063	-0.003	0.003	-0.020	0.07
[Fe/H] II	0.004	0.070	0.009	-0.027	0.08
$\log \epsilon(Li)$	0.072	0.003	0.005	0.000	0.07
[C/Fe] CH	0.067	-0.041	0.036	-0.007	0.09
[N/Fe] CN	0.237	-0.037	0.078	0.020	0.25
[O/Fe] [OI]	0.042	0.004	0.007	0.026	0.05
[O/Fe] OI	-0.079	0.003	-0.013	0.018	0.08
[Na/Fe]	-0.028	0.003	-0.001	0.014	0.03

less luminous than the bump; upper-RGB are RGB stars more luminous than the bump; RGB-bump stars have approximately the luminosity expected for the bump at their metallicity; RHB are stars on the red horizontal branch; and finally AGB is used for a star at the base of the AGB).

Table 4 gives sensitivity of our abundances on the adopted atmospheric parameters for typical giant (HD 2665) and dwarf (HD 194598): these were estimated for variations of the atmospheric parameters within reasonable 1 σ limits. The last column gives an estimate of the total uncertainty, given by the quadratic sum of errors in individual quantities. Values are not given for the ^{12}C/^{13}C ratio because they are very small. In general, most of the error bar stems from errors in the temperatures, which in turn are mainly due to uncertainties in the adopted reddening values; sensitivity to temperatures are somewhat larger for giants than for dwarfs. C and N abundances are also sensitive to the adopted model abundances. Note that O abundances are derived with respect to Fe II: a larger sensitivity on the adopted surface gravity would appears if abundances from Fe I lines were rather adopted.

5.1. Li abundances

Li abundances (Column 4 of Table 5) were obtained by comparison of observed spectra in the region of the resonance doublet at 6707 Å with synthetic spectra. The line list used is the same used by Gratton & D'Antona (1989); wavelengths and gf's of the Li lines are as in Andersen et al. (1984).

Uncertainties in the atmospheric parameters cause errors in Li abundances of 0.07 and 0.12 dex for dwarfs and giants (see Table 4); if we sum quadratically the expected fitting error for the single feature available (~ 0.08 dex), we conclude for typical errors in our Li abundances of ± 0.10 dex for dwarfs and ± 0.14 dex for giants.

5.2. C abundances

We determined carbon abundances (Column 5 of Table 5) and isotopic ratios (Column 12 of Table 5) from synthetic spectra computations of two parts of the CH $A^2\Delta - X^2\Pi$ "G-band". We avoided the prominent $Q-$branch bandhead region from $\approx 4270 - 4330$ Å, because the CH lines in that region are often saturated in our stars (rendering them less sensitive to carbon abundance changes), and because the isotopic splitting between ^{12}CH and ^{13}CH lines is very small (making them useless for ^{12}C/^{13}C determinations). We instead synthesized part of the $R-$ branch (4227-4241 Å) and part of the $P-$branch (4357-4371 Å). These spectral region choices represented our best compromises that maximized CH line density while minimizing other line contamination (for example, avoiding the very strong lines of Ca I at 4226 Å, Sr II at 4216 Å, and Fe I at 4383 Å and 4404 Å).

We adopted initial atomic and molecular line lists in these spectral regions from the Kurucz (1995) database. Initial trial syntheses of solar and stellar spectra demonstrated the ^{13}CH line wavelengths of this database share the systematic offset of ~ 0.20 Å from their laboratory wavelengths that was earlier demonstrated to exist for the ^{13}CH $B^2X - X^2\Pi$ band near 4000 Å (Para 1991; Norris et al. 1997; Westin et al. 1999), and so these wavelengths were altered by this constant amount. We also supplemented the atomic line list to include a few lines identified in the solar spectrum by Moore et al. (1966) but not in the Kurucz database. Finally, a few totally unidentified features in the solar spectrum were arbitrarily assumed to be Fe I lines of 3.0 eV.

We adjusted the initial oscillator strengths of the atomic lines via repeated syntheses of the solar spectrum, but no alteration were made to any CH line oscillator strength. Then we estimated the solar carbon abundance with these line lists. Using our ATLAS solar model atmosphere, comparing our syntheses to the Kurucz et al. (1984) solar atlas, we derived $\log \epsilon(C) = 8.50 \pm 0.05$. This abundance is not to be confused with the recommended $\log \epsilon(C) = 8.60 \pm 0.05$ (Grevesse et al. 1991) which is based on careful consideration of multiple carbon species in the solar spectrum as well as meteoritic results. Our value depends on our particular choices of solar model atmosphere and CH band oscillator strength, but in this way anchors the zero point of the carbon abundances of the programme stars.

We used multiple synthetic spectrum computations to derive carbon abundances and isotope ratios in the programme stars. The carbon abundances were first determined from synthetic/observed spectrum matches with fixed estimated ^{12}C/^{13}C ratios. The initial isotope ratios were assumed to be ^{12}C/^{13}C=40 for MS/TO stars (stars with this or larger isotope ratios have essentially undetectable ^{13}CH lines at our spectral R and S/N values) and 10 for giants (an opening value not too different from previous ratios reported for field metal-poor giants) and several trial choices for the carbon abundance. Then synthetic spectra were computed with the best-fitting total carbon and sev-

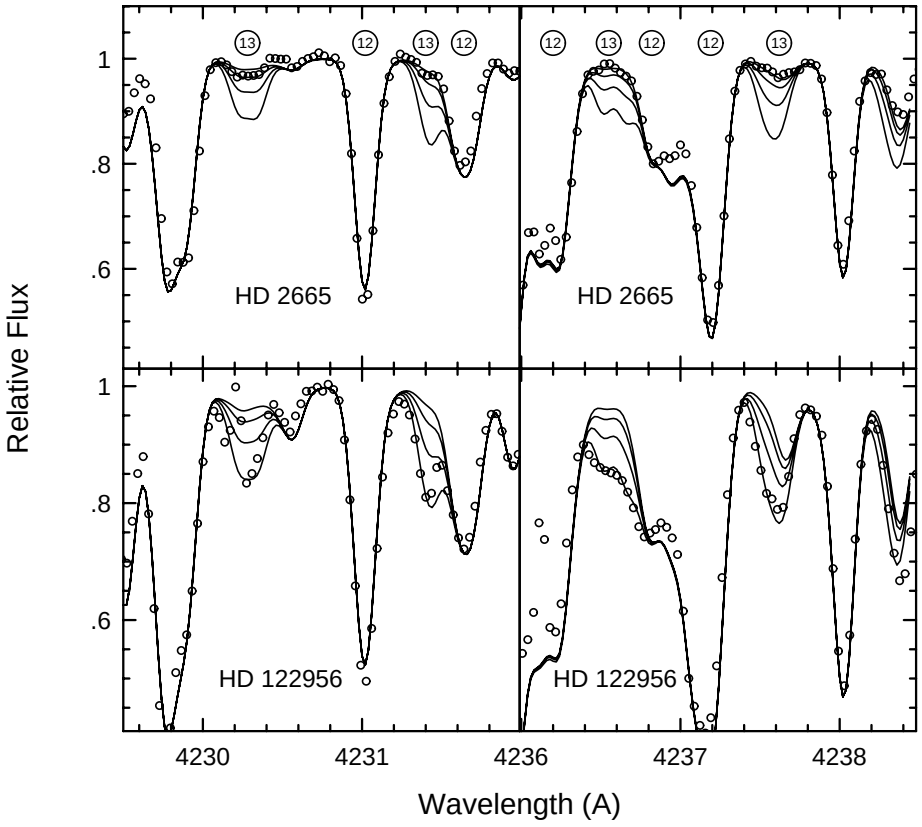

Fig. 5. Comparison between observed and synthesized spectra for two spectral regions within the G-band. The spectral regions showed include part of the $R-$branch. Results for two RGB stars are shown: HD2665 is at the bump luminosity; HD122956 is about 1.5 mag brighter. Observations are small circles. Solid lines are synthetic spectra computed using model atmospheres and C abundances appropriate for the stars, and four different values of the ^{12}C/^{13}C isotopic ratio (5, 10, 20, and 40). Position of ^{12}CH and ^{13}CH lines are shown

eral choices for ^{12}C/^{13}C. The process was repeated until best matches to ^{12}CH and ^{13}CH features were obtained.

Errors in the [C/Fe] ratios are 0.09 dex for dwarfs and 0.10 dex for giants, although errors might be larger for a few stars which do not have accurate atmospheric parameters and/or [Fe/H] values.

In Figs. 5 and 6 we show several small portions of the CH observed and synthesized spectra of HD2665 (a lower-RGB star), and HD122956 (an upper-RGB star). These stars differ by their position on opposite sides of RGB-bump, and the large difference in ^{12}C/^{13}C ratios is easily seen in these spectra.

5.3. N abundances

We determined nitrogen abundances for most stars with McDonald spectra from synthetic spectrum computations of the (0.0) and (1,1) bandheads of the violet $B^2\Sigma^+ - X^2\Sigma^+$ CN electronic transition. The synthetic spectrum covered the wavelength range $3865 \leq \lambda \leq 3885$ Å. We adopted without alteration the atomic and molecular line lists of Kurucz (1995), and chose a dissociation potential of $D_0^0 = 7.59$ eV. The CN dissociation energy is not yet well determined, and values in the range 7.5 to 8.1 eV have been suggested. A brief discussion and references on this issue can be found in Aoki & Tsuji (1997). Since our stellar abundances are tied to the solar value derived with identical CN parameters, the effects of uncertainties in D_0^0(CN) is not large. With this line list and our adopted $\log \epsilon(C)_\odot = 8.50$, we first derived the solar nitrogen abundance in the same fashion as was done for the solar carbon abundance. This exercise yielded $\log \epsilon(N)_\odot = 8.00 \pm 0.10$. We then attempted to synthesize the CN violet bands in the 24 programme stars with McDonald spectra. The derived N abundances merit several cautionary statements: first, some of the bandheads proved to be immeasurably weak in some of the warmest and/or most metal-poor stars (e.g. HD19445, BD+37 1458). Second, there are a few other stars for which the relative weakness of the bandheads severely limits the accuracy of the derived N abundance (e.g. HD45282, HD87140). Third, we repeat the warning issued by other investigators of CN bands: that accuracies of derived N abundances can be no better than the accuracies of the derived (or worse, assumed) abundances of C in each star. Finally, our spectra were not optimized for CN observations, and the S/N of the spectra is somewhat lower than optimal at 3880 Å. Nonetheless, when the CN bands are detectable, derivation of the N abundance is straightforward (see Fig. 7 for a couple of examples); in Table 5 we list our final N abundances.

5.4. O abundances

Oxygen abundances were obtained from both forbidden and permitted lines (Columns 7 and 8 of Table 5 respectively). To reduce sensitivity to the adopted gravities, whenever possible these O abundances were computed with respect to Fe abundances given by ionized lines; however, since on average abundances from Fe II lines agree with those for Fe I lines, no systematic correction to the [O/Fe] results from this procedure. Abundances from permitted lines include (small) corrections for departures from LTE: these were computed according to the prescription given

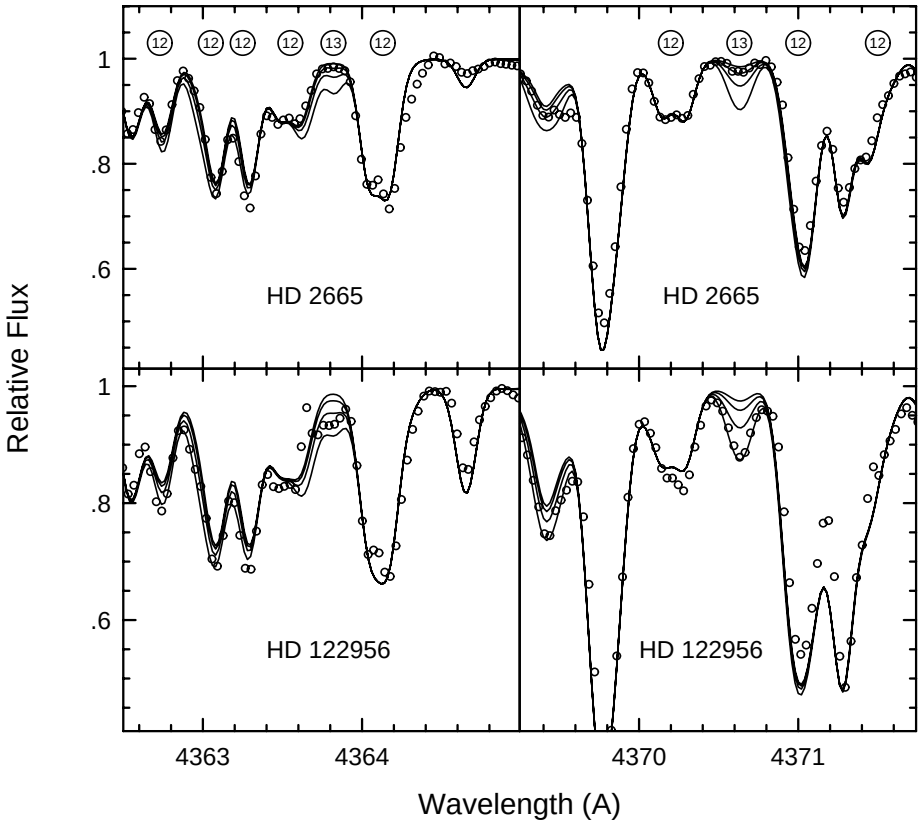

Fig. 6. The same as Fig. 5, but now the spectral regions showed include part of the $P-$branch

by Gratton et al. (1999). These non-LTE corrections are very similar to those estimated by Kiselman (1991); they are small (< 0.2 dex) for all our programme stars. Note that non-LTE corrections are negligible for the forbidden lines. [O/H] values were computed adopting $\log \epsilon(O) = 8.87$, which resulted from an analysis of EW's measured on the solar spectrum by Lambert (1978: [OI]; and Biemont et al. 1991a: permitted lines), and gf's from the same sources, using the Kurucz (1995) solar model. Average [O/Fe] ratios (Column 9 of Table 5) were computed after a small offset of 0.08 dex between abundances from [OI] and O I lines was accounted for (the higher abundances given by the permitted triplet were corrected to those given by the forbidden line). We applied this correction because abundances from the forbidden lines are less sensitive than those from permitted lines on details of the model atmosphere (run of the temperature with optical depth), and to the adopted temperatures.

Combining typical uncertainties in abundances from individual lines with dependences on errors in the atmospheric parameters (see Table 4) we get typical uncertainties in our [O/Fe] ratios of 0.09 dex for dwarfs and 0.12 dex for giants.

5.5. Na abundances

Our Na abundances were derived from the 5682-88 Å and 6154-60 Å doublets [3]; as for O, we also included in our analysis additional EWs from the literature (Sneden et al. 1991; Kraft et al. 1992; Shetrone 1996; Carretta et al. 1999). [Na/H] values assume a solar value of $\log \epsilon(\mathrm{Na}) = 6.23$, which resulted from an analysis of the solar EW's measured by Lambert & Luck (1978), $gf's$ from the same source, and the Kurucz (1995) solar model atmosphere. We give both abundances obtained in a usual LTE analysis, and those obtained including non-LTE corrections, following the prescriptions given in Gratton et al. (1999) (Columns 10 and 11 of Table 5 respectively). These corrections are those appropriate for the lines considered, and take into account line strength. We prefer to give both LTE and non-LTE abundances in this paper because the conceptually superior statistical equilibrium calculations are not yet reliable enough to completely supersede the simpler LTE analysis, even for well studied atoms like O and Na. This is mainly due to uncertainties in the collisional cross sections. The non-LTE corrections of Gratton et al. (1999) were computed using empirical cross sections, calibrated against spectral data for RR Lyrae stars, where non-LTE corrections are expected (and found) to be much larger than in the stars considered in the present paper (due to the combination of higher temperatures and lower gravities), a procedure we deemed more robust than use of very uncertain theoretical estimates. However we emphasize that present non-LTE corrections are small and have only marginal impact on the following discussion. Differences between non-LTE and LTE Na abundances for stars with $-2 <$[Fe/H]< -1 are plotted as a function of luminosity in Fig. 8. Corrections are slightly negative for subdwarfs and subgiants, and become positive for

[3] At the high resolution used throughout this paper, blending of the 5682-88 Å doublet with neighbor lines is not a problem, as verified by appropriate spectral syntheses

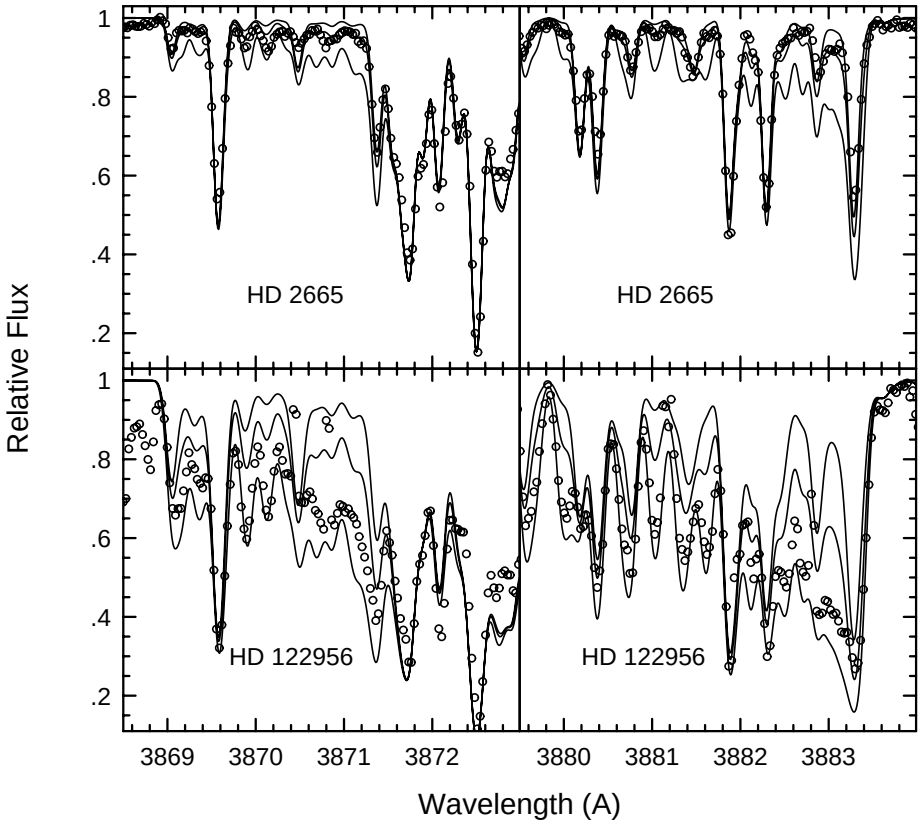

Fig. 7. Comparison between observed and synthesized spectra for (0.0) and (1,1) bandheads of the violet $B^2\Sigma^+ - X^2\Sigma^+$ CN transition. Results for two RGB stars are shown: HD2665 is at the bump luminosity; HD122956 is about 1.5 mag brighter. Observations are small circles. Solid lines are synthetic spectra computed using model atmospheres and C abundances appropriate for the stars, and three different values of the N abundance ([N/Fe]=–0.45, +0.05, and +0.55)

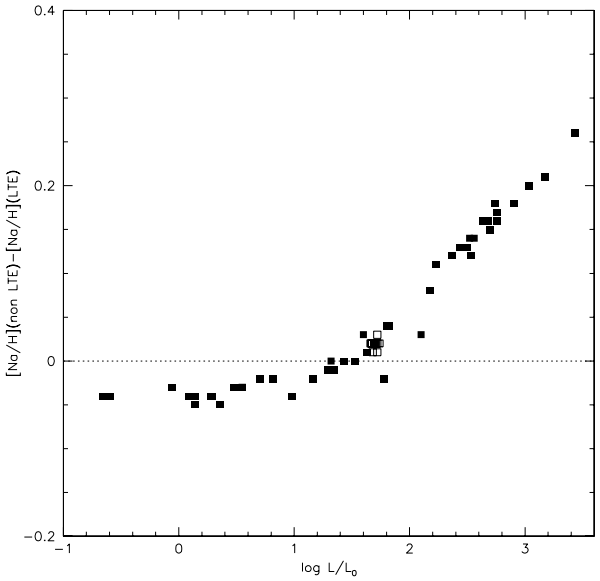

Fig. 8. Non-LTE correction to Na abundances, plotted as a function of stellar luminosities. Filled symbols are MS and first ascent RGB stars. Open symbols are RHB stars

stars brighter than the bump: they are as large as ~ 0.25 dex for stars at the tip of the RGB.

Combining errors in the EWs for the Na lines, with those due to the atmospheric parameters, we arrive at typical errors in the [Na/Fe] ratios of 0.06 dex for dwarfs and 0.08 dex for giants.

6. Additional data

Although our sample is already quite large, we considered improvement in the statistical significance of our results by addition of data from the literature for stars in the ATT list; such a comparison also allows a better discussion of external errors present in our analysis. In order not to confuse observational evidence, a basic requirement is that the additional stars should have accurate [Fe/H], possibly derived from high resolution spectra, and reduced to the system used throughout this paper. In the following, we describe the additional data we used for each of the elements considered in this paper. In Table 6 (only available in electronic form) we give the final set of abundances used in our discussion; these were obtained by combining those of Table 5 with the literature data described below. The total sample consists of 105 stars, 70 of them with $-2 <$[Fe/H]< -1.

6.1. Lithium

We have 14 stars in common with Pilachowski et al. (1993). Our effective temperatures are on average higher by 112 ± 32 K (with a rather large scatter of 120 K for individual stars). Not surprisingly, we found higher Fe and Li abundances (by 0.09 ± 0.03 and 0.21 ± 0.03 dex respectively). However, the star-to-star scatters are quite small ($\sigma = 0.10$ dex for both Fe and Li). These small scatters make it possible to merge the two samples, in order to have a large sample of metal-poor stars with Li abundances. Combining the two samples, Li abundances are available for 70 stars, 48 with $-2 <$[Fe/H]< -1.

6.2. Carbon

Three extensive sets of C abundances for field metal-poor stars have been published. Kraft et al. (1982) and Carbon et al. (1987) derived C and N abundances from a comparison of low resolution ($R \sim 500$) image dissector scanner spectra of the CH and NH bandheads, with synthetic spectra computed using the Bell et al. (1976) model atmospheres. Their sample includes about 150 stars. Their data clearly show a decline of C abundances with increasing stellar luminosity, although less pronounced than for globular cluster stars of similar metallicity (Langer & Kraft 1984); on average this result agrees well with ours. A star-to-star comparison shows however a considerable scatter in the [C/Fe] values ($\sigma = 0.21$ dex, 16 stars in common), not unexpected in view of the quality of the observational material used in this earlier investigations: in fact, it is not much larger than the error estimated by the authors (0.15 dex). However, this error bar is large enough so that addition of their data to our sample does not help to improve our understanding of the mixing episodes along the RGB.

A similar conclusion is reached by comparing our C abundances with the analysis of 116 field metal-poor dwarfs by Laird (1985). Laird's analysis is based on low resolution ($R \sim 1500$) image tube spectra: the lower S/N of these spectra explains the larger scatter with our data (0.25 dex, 9 stars). Note however that the main conclusion reached by Laird (a nearly constant [C/Fe] with decreasing [Fe/H] in unevolved stars; see also Carbon et al. 1987) is well supported by our analysis.

On the other hand, we found a small star-to-star scatter ($\sigma = 0.09$ dex, 13 stars) when comparing our [C/Fe] with those obtained recently by Rossi et al. (1999) from moderate resolution ($R \sim 1500$), high S/N CCD spectra of 91 metal-poor stars; note that this low σ value was obtained after exclusion of two outliers (HD105546 and BD+37 1458). Rossi et al.'s $\log \epsilon(C)$ values agree very well with ours: the offset is only 0.02 ± 0.03 dex[4]. This impressive agreement allowed us to combine their C abundances with ours, without any systematic correction, although the existence of a few outliers warn us about the possibility that errors are much larger than average for a few stars. To keep the sample as homogeneous as possible, metallicities for the additional stars were obtained using data reduced to the scale used in the present paper (these were not available for several stars in the Rossi et al. sample); luminosities were derived from ATT. In total, we have C abundances for 86 stars, 56 of them with metallicities in the range $-2 <$[Fe/H]< -1.

6.3. Oxygen

O abundances for additional stars in the ATT list (mainly giants) were obtained using EW's for forbidden lines gathered from the literature. This increase in sample size allows a better discussion of abundance spreads along the evolutionary sequence, and then a better comparison with results for globular clusters. We used data from Gratton and Ortolani (1986), Barbuy (1988), Sneden et al. (1991), Kraft et al. (1992), Shetrone (1996), and Carretta et al. (1999). Results from the four latest analysis were preferred, since they are based on better observational material (data in the oldest papers were obtained using a Reticon detector, not as well suited for faint star observations as CCDs). We performed an analysis essentially identical to that done for the programme stars; however Fe abundances were those from the original sources, systematically corrected for the offsets with the present determinations (as determined from the stars in common with the various samples). In total, data were available for 78 stars, 53 with $-2 <$[Fe/H]< -1.

There are several oxygen abundance determinations for samples of metal-poor stars in the literature. Our [O/Fe] agrees very well with previous determinations from the [OI] lines (Gratton & Ortolani 1986; Barbuy 1988; Spite & Spite 1991; Sneden et al. 1991; Kraft et al. 1992). More intriguing are comparisons with papers which made use of the OI IR triplet and of the OH band in the UV. We will consider here three recent papers which used these features.

Cavallo et al. (1997) performed an LTE analysis of the OI IR triplet of dwarfs and subgiant stars. There are 8 stars in common with our sample, but for two of them we did not measure EW's of triplet lines. On average, the EWs agree fairly well (mean difference is 1.8 ± 0.8 mÅ, with $\sigma = 3.6$ mÅ). There are however large differences in the atmospheric parameters: our $T_{\rm eff}$'s and $\log g$'s are higher on average by 106 ± 50 K and 0.29 ± 0.10 dex, with large star-to-star scatter (141 K and 0.28 dex respectively). As expected from these differences, Cavallo et al.'s [Fe/H] values are lower than ours (on average by 0.14 ± 0.07 dex). LTE [O/H] values are quite similar (offsets due different temperature and gravity scale roughly cancel out); however, our finally adopted [O/H] values are smaller, due to the non-LTE corrections (~ 0.15 dex on average). Summarizing, our [O/Fe] values from the triplet lines are smaller than those by Cavallo et al. by 0.32 ± 0.13 dex for two reasons: the [Fe/H] values are larger (due to the higher $T_{\rm eff}$ scale adopted), and we consider small non-LTE corrections.

Israelian et al. (1998) used the UV OH band to derive O abundances in a number of dwarfs and a few subgiants. This technique is very interesting, since the OH band can be measured even in very metal-poor stars. They have 8 stars in common with our analysis, and their [O/Fe] values are larger than ours by 0.31 ± 0.05 dex ($\sigma = 0.15$ dex). The atmospheric parameters used by Israelian et al. are systematically different from those of this paper: $T_{\rm eff}$'s and $\log g$ are larger by 130 K and 0.27 dex respectively, with a remarkably small star-to-star scatter ($\sigma =$ 49 K and 0.08 dex respectively). They did not derive new [Fe/H] values, but rather gathered them from the literature: they are on average lower than ours by 0.23 dex (again, the scatter is small: $\sigma = 0.10$ dex). This difference cannot be justified simply by the lower temperatures; an analysis of Fe abundances similar to that done in this paper, but with their atmospheric parameters, would have produced Fe abundances larger than those used by Israelian et al. by 0.15 dex: this accounts for half the difference in

[4] Note that although Rossi et al. synthesized the entire 4200-4400 CH G-band spectral region, the largest weight in their derived abundances came from the strong $Q-$branch lines near 4300 Å, while our abundances are from $P-$ and $R-$branch weaker features

[O/Fe] values. The [O/H] values of Israelian et al. are on average higher than ours by 0.10 ± 0.05 dex. Since we used higher $T_{\rm eff}$'s, $\log g$'s, and [Fe/H]'s, we would expect their [O/H] values to be 0.12 dex lower than ours. There is then an offset of 0.22 dex.

Boesgaard et al. (1999) have also recently performed an analysis of the OH band for metal poor dwarfs. There are 8 stars in common with our sample; however we leave out from this comparison HD219617, which gives very discordant results. They give results obtained with two sets of model atmospheres parameters: the "King" ones are very similar to ours (offset in $T_{\rm eff}$'s and $\log g$'s are 3 ± 27 and 0.05 ± 0.05 dex respectively, our values being lower), so that results of the abundance analysis can be directly compared. Boesgaard et al. do not derive [Fe/H] values; their discussion of the literature gives values a bit lower than ours (0.08 ± 0.02 dex): this difference may be attributed to a different reduction to the solar abundance. The [O/H] abundances they obtained from an LTE analysis of the OI triplet are very consistent with ours (our values are lower because we included non-LTE corrections); however, those obtained from OH lines are higher than ours by 0.20 ± 0.05.

Both analysis based on the OH band gives then O abundances larger than those given by [OI] lines by about 0.2 dex. However, gf's for the OH bands are uncertain, and in both analyses they were adjusted in order to fit the solar spectrum with the solar abundance of $\log \epsilon(O) = 8.93$ given by Anders & Grevesse (1989). This fit is uncertain due to difficulties in the location of the continuum level in this very crowded spectral region: it is then possible that systematic offsets exist in these abundance analyses.

Summarizing, all these papers obtained higher abundances than those obtained from the [OI] lines. However, from Table 4 it is clear that abundances from [OI] lines are less affected than those from the OI triplet by uncertainties in the adopted parameters; furthermore, they form in LTE. Finally, EW's for the forbidden lines may be accurately measured even in metal-rich stars (e.g. in the Sun) and gf's are well known (both these effects may be a concern for the UV OH band). For this reason we give higher weight to abundances derived from the [OI] lines.

6.4. Sodium

Pilachowski et al. (1996) obtained Na abundances for 60 metal-poor field giants. Eleven stars are in common with our sample. On average, the [Fe/H] they obtained for these stars are lower than ours by 0.04 ± 0.05 dex ($\sigma = 0.15$ dex): a star-to-star comparison shows that this difference is due to different assumptions about effective temperatures (mainly related to uncertainties in the adopted reddening) and microturbulent velocities (derived from only a few lines available): once these differences are taken into account, the two sets of data agree very well. The [Na/H] values (derived from the 5682-88 Å doublet) are less sensitive to details about the atmospheric parameters, and correlate very well with our abundances, with a mean offset of 0.19 ± 0.03 dex ($\sigma = 0.10$ dex). This offset is due to the different procedure adopted to compare stellar and solar abundances: absolute abundances $\log \epsilon({\rm Na})$ agree very well within the noise.

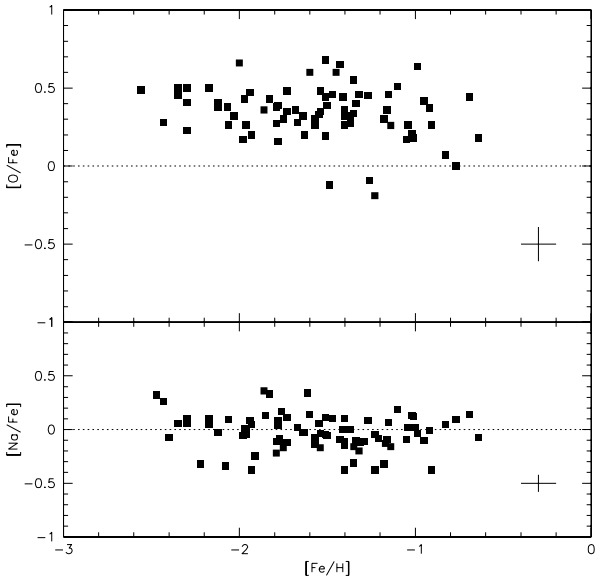

Fig. 9. Run of the [O/Fe] and [Na/Fe] abundance ratios with overall metallicity. Typical error bar is shown at bottom right of each panel. No clear trend with overall metallicity is apparent, supporting the hypothesis that initial mixture of metals was the same for almost all the programme stars. A few stars with negative [O/Fe] ratios are discussed in the text

Given the good correlation between Pilachowski et al. (1996) and our Na abundances, we may combine the two samples, provided that the offsets between the two sets of abundances are taken into account. Here we could not derive new homogeneous abundances from the EWs, as it was done for O, because Pilachowski et al. did not measure EWs for the Na lines, but rather compared the observed spectra with synthesized ones. We also could not evaluate the non-LTE corrections for individual lines; so for this comparison we first normalized the LTE Fe and Na abundances from Pilachowski et al. to our scale. Non-LTE corrections were then estimated using a smooth curve through the well defined relation of Fig. 8. In this way we obtained a large sample of 92 metal-poor stars (63 with $-2 <$[Fe/H]< -1), having accurate absolute magnitudes determined uniformly by ATT and [Na/Fe] ratios with typical errors of $\sim \pm 0.10$ dex.

7. Discussion

7.1. Primordial abundance spread

A basic assumption behind our description of the evolution of elements along the RGB is that stars shared the same initial mixture of heavy elements. While this assumption might sound appropriate for a cluster, it could well be wrong for field stars, either due to systematic trends of abundance ratios with [Fe/H] (as suggested for O by recent results based on OH in the near UV: Israelian et al. 1998; Boesgaard et al. 1999), or to star-to-star variations at a given [Fe/H]. The last effect is widespread amongst the most metal-poor stars ([Fe/H]< -2: see e.g. McWilliam et al. 1995); however the ISM seems reasonably well mixed

when metallicities are above [Fe/H]> -2, so that most stars in the metallicity bin considered here may be assumed to have the same initial mixture of the elements. To confirm this, in Fig. 9 we plotted the abundance ratios [O/Fe] and [O/Fe] against overall metal abundance [Fe/H] for all stars studied in this paper (even those outside the range $-2 <$[Fe/H]< -1). No trend can be discerned, and the scatter is generally consistent with observational errors, save for the most metal-rich stars ([Fe/H]> -1) where some contamination by disk stars becomes apparent. The larger than average Na abundances in the most metal-poor stars ([Fe/H]< -2.2) are based on a few very weak features and should be confirmed by very high S/N observations. While the absence of trends cannot be considered as a conclusive result for all metal-poor stars (data are sparse for stars with [Fe/H]< -2, and our sample covering a wide range in luminosity was not appropriately selected for this purpose), it shows however that our basic assumption of uniform initial mixtures of elements may be considered a quite safe hypothesis for the abundance range we are mainly concerned with ($-2 <$[Fe/H]< -1), at least at the level of accuracy of ± 0.1 dex.

We found three stars with subsolar O abundances: HD 134439, HD 219617, and BD+30 2611. The two first stars are subdwarfs, while the third one is a bright giant. The low O abundances for HD 134439 and BD+30 2611 were previously noticed by King (1997) and Kraft et al. (1992). Boesgaard et al. (1999) obtained an O abundance much higher than ours for HD 219617, so we think this star should be reobserved with more extensive data than used here (only a few CAT spectra were available for this star). Of these stars, only BD+30 2611 is evolved enough for any significant mixing to occur; however this star is not the counterpart of the O-poor, Na-rich stars found in several globular clusters (Kraft 1994), since it also has a low Na abundance. Rather, the low O abundance of this star seems related to its initial composition, or to errors in the Fe abundance. In fact, other $\alpha-$elements (Mg and Ca) are also low in this star (Kraft et al. 1992; Pilachowski et al. 1996; Shetrone 1996). A further argument against mixing in this star is the low N abundance found by Carbon et al. (1982) (if surface O abundances are altered by deep envelope mixing of complete CNO cycle products, N surely would also be brought to the surface). We will omit these stars from further consideration about mixing episodes along the RGB, since they seem not to share the same initial mixture of heavy elements, typical of the other stars in the metallicity bin considered in this paper.

7.2. Mixing episodes along the RGB

The mixing episodes along the RGB are described very well by the runs of the abundances of the most fragile elements (Li and ^{12}C), and of the ^{12}C/^{13}C isotopic ratios. Additional data are provided by N abundances.

In Fig. 10 we have plotted the runs of the abundance of Li, of the abundance ratios [C/Fe], [N/Fe], [O/Fe], and [Na/Fe], and of the isotopic ratio ^{12}C/^{13}C with luminosity for stars with $-2 <$[Fe/H]< -1. Filled symbols are actual measures; arrows are upper (for Li) or lower (for ^{12}C/^{13}C) limits. Dashed lines separate various evolutionary phases (MS and TO stars; lower-RGB stars; upper-RGB stars). Results for RHB stars are plotted separately for clarity. Table 7 gives average values of the abundances in these different evolutionary phases for stars in the same abundance bin. These are obtained after eliminating a few discrepant stars discussed below.

First consider lithium abundances. Here our results are essentially identical to those of Pilachowski et al. (1993). Our Li abundance for main sequence stars is $\log \epsilon(Li) = 2.40 \pm 0.04$ (this is the value for stars with $\log L/L_{\odot} > -0.2$, that are on the so-called Spite plateau: Spite & Spite 1982). This value is higher than the usually assumed value (see e.g. $\log \epsilon(Li) = 2.24 \pm 0.01 \pm 0.05$: Bonifacio & Molaro 1997). This is due to our adoption of higher effective temperatures for the programme stars than done by most other authors. We do not consider this difference as important here, because we are mainly concerned with the evolution of surface abundances rather than in the absolute abundances of elements. The star with the highest Li abundance in our sample is BD+23 3912 (this is also the star with the highest Li abundance in the Pilachowski et al. sample; note that the Li abundance for this star used here is derived from our McDonald spectra, and it is thus independent from Pilachowski et al.): it has also been suggested that this star might have a Li abundance higher than that typical of the Spite plateau (King et al. 1996). In the luminosity range of the Spite plateau we also found two stars with low Li abundances (HD 196892 and HD 199289). These last two stars were not considered in our average. When the convective envelope expands inward (roughly, when the first dredge-up occurs, at a luminosity of $\log L/L_{\odot} \sim 0.8$ for stars in our bin of metallicity), the surviving Li in the outer convective shell is diluted. This results in a decreased surface abundance that is quite progressive in effective temperature (see Figs. 7 and 8 of Pilachowski et al. 1993), but rather abrupt in luminosity (see our Fig. 10). Then the surface Li abundance stabilizes along the lower-RGB, at an average value of $\log \epsilon(Li) = 1.15 \pm 0.03$. The dilution factor we found is slightly less than a factor of 20, in good agreement with previous observational data and theoretical models (Pilachowski et al. 1993). However, when the expanding H-burning shell reaches the discontinuity left by the maximum inward penetration of the convective shell (at a luminosity of $\log L/L_{\odot} \sim 2.0$ for stars with $-2 <$[Fe/H]< -1), practically all remaining Li is destroyed: we did not detect the Li line in any upper-RGB stars and RHB-stars save for HD41667 and HD122956 that are the faintest upper-RGB stars in our sample, and one up-RGB star (HD118055); even for these stars, only weak Li lines were detected, yielding a very low value of $\log \epsilon(Li) \leq 0.0$. Our data clearly indicate that when the $\mu-$barrier is canceled, Li is destroyed.

Turn now to carbon. In unevolved stars ($\log L/L_{\odot} < 0.8$), the average C abundance in the metallicity bin here considered is [C/Fe]$=-0.09 \pm 0.02$, based on 15 stars, with $\sigma = 0.08$ dex. While our main goal is not to determine the run of the C abundance with [Fe/H], we note that our slightly negative value agrees well with earlier investigations (Laird 1985; Carbon et al. 1987; Tomkin et al. 1992). In agreement with theoretical

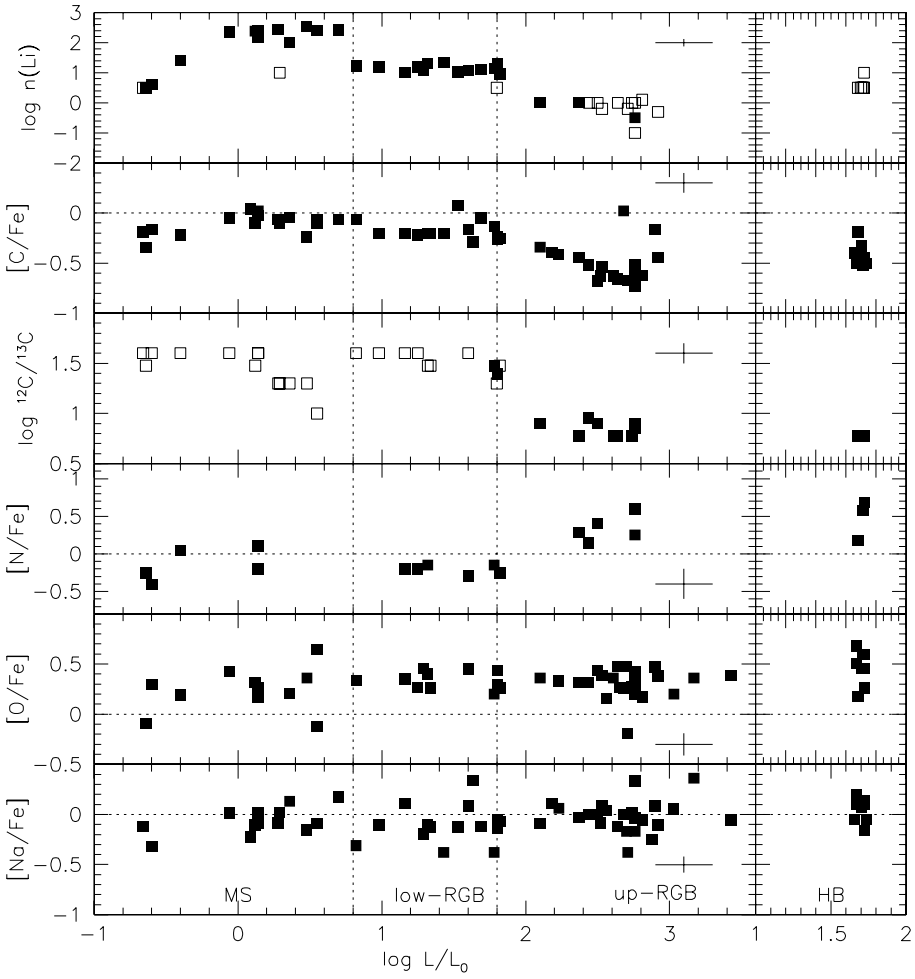

Fig. 10. Run of the abundance of Li, of the abundance ratios [C/Fe], [N/Fe], [O/Fe] and [Na/Fe], and of the isotopic ratio $^{12}C/^{13}C$ with luminosity for stars with $-2 <$[Fe/H]< -1. Filled symbols are actual measures; arrows are upper (for Li) or lower (for $^{12}C/^{13}C$) limits. Typical error bars for the various quantities are shown. Dahed lines separate various evolutionary phases (MS and TO stars; lower-RGB stars; upper-RGB stars). Results for RHB stars are plotted separately for clarity

Table 7. Average abundances in different evolutionary phases for stars with $-2 <$[Fe/H]< -1

Element	MS and TO			lower-RGB			upper-RGB			RHB		
$\log\epsilon(Li)$	12	2.40 ± 0.04	0.10	13	1.15 ± 0.03	0.12		< 0.0			< 0.0	
[C/Fe]	15	-0.09 ± 0.02	0.08	14	-0.14 ± 0.03	0.11	15	-0.58 ± 0.03	0.12	7	-0.44 ± 0.05	0.14
[N/Fe]	4	-0.11 ± 0.12	0.23	6	-0.21 ± 0.02	0.06	8	$+0.39 \pm 0.07$	0.21			
[O/Fe]				16	$+0.34 \pm 0.03$	0.12	21	$+0.34 \pm 0.02$	0.09	8	$+0.47 \pm 0.06$	0.17
[Na/H]				25	-0.09 ± 0.03	0.15	22	-0.02 ± 0.03	0.15	10	$+0.05 \pm 0.03$	0.11

computations (VandenBerg & Smith 1988; Charbonnel 1994), the C abundance declines only marginally at first dredge up: we obtain an average value of [C/Fe]$=-0.14 \pm 0.03$, based on 14 stars on the lower-RGB, with $\sigma = 0.11$ dex. While the difference of 0.05 dex between MS and lower-RGB C abundances coincides with theoretical expectations, this difference is small and not statistically significant.

A much more significant decrease of the C abundance occurs when stars evolve off the RGB-bump: the average value for our group of upper-RGB stars is [C/Fe]$=-0.58 \pm 0.03$ (15 stars). While the σ is quite low in the [C/Fe] ratios of upper RGB stars (0.12 dex), systematic trends are still present within this group. We in fact obtained the lowest [C/Fe] ratios for the most evolved and/or most metal-poor stars in this group (however there is a large spread in the [C/Fe] ratios for stars with [Fe/H]< -2; see below). Metallicity might play a role: while the average value of the [C/Fe] ratio for upper-RGB stars is even lower than that provided by more evolved RHB stars ([C/Fe]$=-0.44 \pm 0.05$, 7 stars with $\sigma = 0.14$ dex), these two groups of stars seem to follow a similar correlation between [C/Fe] and [Fe/H] (see lower panel of Fig. 11, where also stars out of the metallicity range considered in the present discussion are plotted). A metallicity dependence of deep mixing along the RGB was indeed predicted by Sweigart & Mengel (1979), although no clear quantitative prescription could be given on the basis of their models alone. From Fig. 11 we see that mixing might apparently be a function of metallicity, being less efficient in more metal-rich stars and reaching a maximum value for [Fe/H]~ -1.5. Similar results are obtained using the N abundances, although for this element the result has less statistical strength due to the small number of

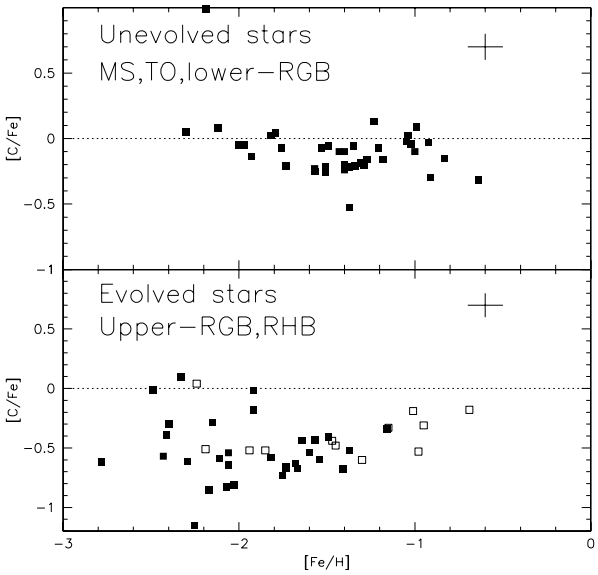

Fig. 11. Run of the [C/Fe] abundance ratio with [Fe/H] for unevolved stars (i.e. stars less luminous than the first dredge-up), and evolved ones (i.e. stars evolved off the RGB-bump: filled symbols are upper-RGB stars, and empty ones are RHB stars)

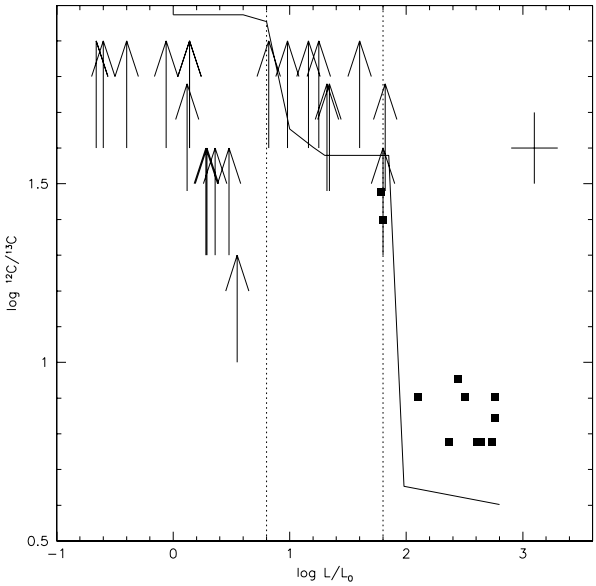

Fig. 12. Run of the isotopic ratio ^{12}C/^{13}C with luminosity for stars with -2 <[Fe/H]< -1. Filled symbols are actual measures; arrows symbols are lower limits. Superimposed is the evolutionary sequence for a 0.8 $M_\odot$ star with $Z = 10^{-3}$ experiencing a rotationally-induced deep mixing (Charbonnel 1995)

stars for which data are available. The observed star-to-star scatter is small for [Fe/H]> -1.9, suggesting that the mechanism responsible for this mixing is quite universal. At metallicities below [Fe/H]≤ -1.9 a large scatter in [C/Fe] is observed for stars evolved off the RGB bump. However, since we have no unevolved stars at these low metallicities, it is not clear if this larger scatter is due to a scatter in the original element-to-element abundances (as observed for several elements by McWilliam et al. 1995), or rather to some factor modulating mixing efficiency.

In the case of the ^{12}C/^{13}C isotopic ratio the variation in the isotopic ratio at the bump luminosity is obvious in our spectra: it can be easily seen by comparing the spectral region including the CH lines for stars within the RGB-bump (like HD2665) and slightly above it above (like HD 122956: see Figs. 5 and 6). ^{13}CH lines are at most barely detected in the spectrum of the bump star HD2665, while they are clearly visible in the spectra of the upper-RGB star HD122956. While this result is typical for the programme stars, this particular pair shows that the change in surface abundance occurs in a short interval after the RGB-bump. A more quantitative comparison with models is also possible, since we may compare our results with the predictions by Charbonnel (1995) for a 0.8 $M_\odot$ star with $Z = 10^{-3}$ (Fig. 12). According to these models (that roughly match the stars in our metallicity bin), first dredge-up occurs in the luminosity range $0.8 < \log L/L_\odot < 1.0$, and lowers the ^{12}C/^{13}C from the original value (assumed to be solar) down to ~ 40. This value agrees with our lower limits. In the Charbonnel models, further rotationally induced mixing occurs after the H-burning shell contacts the chemical discontinuity left by the maximum inward penetration of the convective shell; for the particular model here considered, this occurs at a luminosity slightly higher than $\log L/L_\odot \sim 1.8$: this prediction also

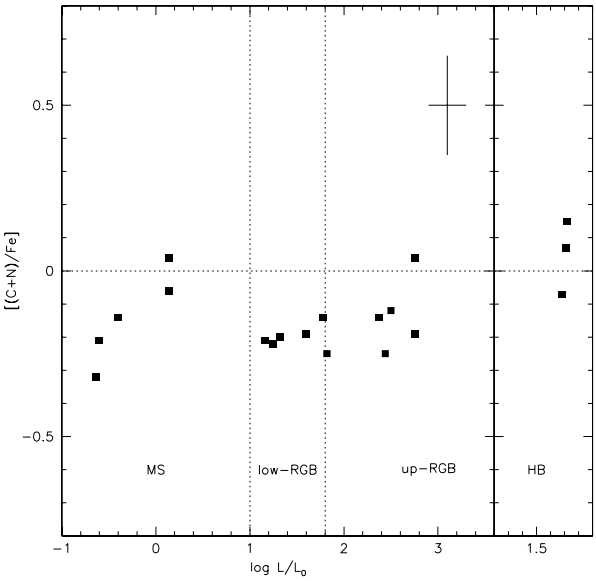

Fig. 13. Run of the ratio of the sum of C and N abundances with luminosity for stars with -2 <[Fe/H]< -1. Expected error bar is also shown

agrees very well with our observations. In the Charbonnel models, the ^{12}C/^{13}C ratio reaches approximately the equilibrium value of the CNO cycle at brighter luminosities: this value is a bit lower than given by our data. That is, deep mixing is somewhat less efficient than given by the models. In spite of this small difference, we regard our observations as a clear confirmation that a second mixing episode occurs just where the Charbonnel models predict.

While N abundances are available for only a few stars, and their error bars are significantly larger than for the other elements, they essentially confirm the picture drawn from Li and C abundances. We find a very mild deficiency of N in unevolved stars ([N/Fe]=-0.11 ± 0.12 dex for 4 stars with $-2 <$[Fe/H]< -1). While this result cannot be considered as conclusive (few stars were observed, error bars are quite large), it agrees with previous investigations of N abundances from unevolved, metal-poor stars (Laird 1985; Carbon et al. 1987). The first dredge-up has no significant effect on the N abundances, confirming the result found for C and theoretical predictions: the abundances we found for MS and TO stars agree within the quite large error bar with those obtained for lower-RGB stars. Errors are large enough to mask the small change of ~ 0.1 dex predicted by models, so that it is not clear if our data confirms this theoretical prediction. In contrast, upper-RGB and RHB stars show large N-excesses (we put these two groups together in Table 7 to improve statistical significance of our result for N); the average value of [N/Fe] for these stars is [N/Fe]=0.39 ± 0.07. The abrupt rise of the N abundance (about a factor of four) when stars evolve-off the RGB bump is obvious in Fig. 10. This is a mixing effect involving regions where CN-burning occurs. In fact, the sum of the Carbon and Nitrogen abundances remains constant (see Fig. 13); the average values for stars below and above the RGB bump are [(C+N)/Fe]=-0.16 ± 0.03 (10 stars, $\sigma = 0.09$ dex) and -0.06 ± 0.05 (8 stars, $\sigma = 0.14$ dex) respectively.

Summarizing, abundances of Li, ^{12}C, and ^{13}C and ^{14}N change abruptly at a luminosity very similar (likely identical) to that of the RGB bump. This demonstrates the existence of a second mixing episode along the RGB, which is active after the molecular weight barrier is canceled. Almost all stars in our sample which are evolved off the RGB bump show very low ^{12}C abundances and ^{12}C/^{13}C ratios, high N abundances, and no detectable Li: this second mixing episode is then the result of the normal evolution of single, isolated stars along the RGB.

7.3. The Na-O anticorrelation in field giants

A possible interpretation of the Na-O anticorrelation seen amongst globular cluster stars is that the mixing episode occurring along the upper-RGB might be very deep, reaching the ON-burning shell (for references, see Kraft 1994). Is the mixing episode observed in field halo stars also so deep? On this point, model predictions are not clear. According to Sweigart & Mengel (1979), such deep mixing is possible only for low metallicity values, and only for the more rapidly rotating stars; however, it is not obvious that field and cluster stars have systematically different rotation. Observations obtained before this paper (e.g. Kraft et al. 1982; Shetrone 1996; Pilachowski et al. 1996; Kraft et al. 1997) did not find evidence for such deep mixing for field stars, pointing toward a systematic difference between field and cluster stars. However, the samples of upper RGB field giants, considered in these previous investigations were not as numerous as those obtained for globular clusters, so that some residual concern might still exist.

With our large sample we discuss this issue anew. Homogeneous O abundance determinations are available for 75 stars, 50 of them with $-2 <$[Fe/H]< -1. [O/Fe] ratios are plotted against luminosity in Fig. 10. No obvious trend can be discerned. Average O abundances are essentially the same in different evolutionary phases, when a few discrepant cases discussed in Sect. 7.1 are eliminated: [O/Fe]=$+0.34 \pm 0.03$ dex in lower-RGB stars (16 stars, $\sigma = 0.12$ dex); [O/Fe]=$+0.34 \pm 0.02$ dex in upper-RGB stars (21 stars, $\sigma = 0.09$ dex); [O/Fe]=$+0.47 \pm 0.06$ dex in RHB stars (8 stars, $\sigma = 0.17$ dex). Four additional stars with luminosity very close to the bump yielded a mean [O/Fe] ratio of [O/Fe]=$+0.30 \pm 0.05$ ($\sigma = 0.10$ dex). Finally, we obtained [O/Fe]=+0.55 for HD215601, a star at the base of the AGB judging from the ATT data. Scatter around the mean values for these stars is compatible with observational errors, estimated to be about 0.09 dex for MS and TO star, 0.12 for RGB stars, and somewhat larger (~ 0.15 dex) for the warmer RHB stars since in these spectra, very few Fe lines could be measured on the CAT spectra (only three RHB stars, HD6229, HD105546, and HD166161, have better McDonald spectra).

In Fig. 10 we also plotted the [Na/Fe] ratios for individual stars against stellar luminosity. The data in this figure give little margin for a significant modification of the Na abundance in field stars while stars climb up the RGB. In fact, abundances for stars below and above the RGB bump appear to be similar: on average, we have [Na/H]=-0.09 ± 0.03 (25 stars, $\sigma = 0.15$ dex) and -0.02 ± 0.03 dex (22 stars, $\sigma = 0.15$ dex) respectively. Five stars at luminosities very near the bump have an average value of [Na/H]=-0.17 ± 0.05 dex (r,m,s=0.12 dex). These values are very similar each other. Numbers change slightly (but not this basic conclusion) if LTE abundances are considered instead: in this case we have [Na/H]=-0.07 ± 0.03 and -0.17 ± 0.03 dex respectively for stars below and above the clump. Slightly larger average [Na/Fe] values are obtained for the 10 RHB stars with $-2 <$[Fe/H]< -1 present in this sample: in this case the average [Na/Fe] value is $+0.05 \pm 0.03$ dex ($\sigma = 0.11$ dex); the value is $+0.03 \pm 0.03$ when LTE abundances are considered.

Summarizing, our data show no clear signs of evolution of the [Na/Fe] along the RGB for field stars, in analogy with the result found for O: typical scatter (0.14 dex) is somewhat larger than expected, and that may hint at the presence of a real small star-to-star scatter. However there is no sign of a Na-O anticorrelation in our data, at variance with the results for globular clusters. This is shown in Fig. 14, where we compare the O-Na anticorrelation obtained from stars in M13 (admittedly, an extreme case for the Na-O anticorrelation: see Kraft 1994) with those from stars in our field sample; to make the comparison more significant, we only plotted those field stars which have evolved off the RGB clump (either upper-RGB stars, filled symbols, and RHB stars, empty symbols). To avoid confusion due to possible trends in the abundance ratios with [Fe/H], we only considered stars in the metal abundance range $-2 <$[Fe/H]< -1: this range is approximately centered on the metal abundance of M13 ([Fe/H]=-1.58: according to Kraft et al. 1997; -1.39: following Carretta & Gratton, 1997, whose scale is consistent with that used in this paper). The two samples have comparable size

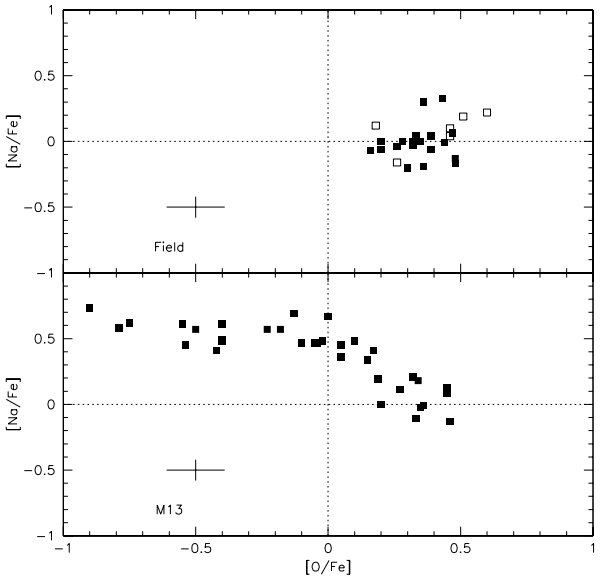

Fig. 14. The Na-O anticorrelation for field stars and for stars in M13. Filled symbols are stars first ascending the RGB (only upper-RGB stars are shown); open symbols are RHB stars. Error bars are shown at bottom left

(29 field stars vs 34 stars in M13), so that a visual inspection gives a nearly correct impression of the real distribution in the two samples. The comparison is striking: within our field sample, no star has [O/Fe]< 0 (the minimum value is much higher than this limit, at [O/Fe]=+0.16: HD 8724), while more than half of the bright giants in M13 (18 out of 34) have [O/Fe]< 0. While the scatter for field stars is compatible with observational errors alone, at about 0.1 dex, the [O/Fe] values for M13 quite uniformly fill the range -1 <[O/Fe]< 0.5. The conclusion reached in earlier analysis (Kraft 1994; Pilachowski et al. 1996; Shetrone 1996; Hanson et al. 1998) of a clear difference between field and cluster stars is strengthened by the present results. We do not regard as important the fact that slight trends of [Na/Fe] abundances with luminosities have been found in other (LTE) analysis (see e.g. Pilachowski et al. 1996), but not in ours, since this difference can be attributed to the different model atmospheres adopted, and to small systematic differences in the atmospheric parameters.

We conclude that the mixing episode occurring at or after the RGB bump is not deep enough in field stars to bring to the surface a significant amount of material processed through complete CNO cycle.

7.4. Discordant stars

We comment finally about a few discordant objects, left out from the previous discussion:

- HD3008: This star has been noted to have a strong G-band by Bond (1980). and it is a binary according to Carney & Latham (1986)
- HD25329: Wilson (1962) first noticed the strong CN bands of this star, and Harmer & Pagel (1973) identified this as an N-rich dwarf (later confirmed by Laird 1985, and Carbon et al. 1987). Our N abundance is very high ([N/Fe]=1.00). The [C/Fe] ratio is the largest for the whole sample ([C/Fe]=+0.11). Beveridge & Sneden (1994) found a high O abundance and a solar Ba/Eu ratio. These facts together suggest that the outer layers of this MS star contain the products of both triple$-\alpha$, CN burning, and $s-$process element production. The most likely explanation for this abundance pattern is pollution by an intermediate mass star undergoing thermal pulses and some hot bottom burning. However, no direct evidence has been found insofar for a companion
- HD93529: the temperature adopted in our reanalysis of this star is about 200 K higher than the temperature adopted by Pilachowski et al. (1996). Use of a lower temperature would result in abundances in better agreement with the star's luminosity
- HD134439: this is an O- and $\alpha-$element poor halo star (King 1997). We confirm the low O abundance (our value is [O/Fe]=-0.09) and find C and N abundances to be low also ([C/Fe]=-0.34; [N/Fe]=-0.25)
- HD135148: we found an anomalously large C abundance for this upper-RGB star ([C/Fe]$= -0.02$). A similar result has been found by Kraft et al. (1982) who define this star as "a cool star with a strong G-band". Note that this star is a binary according to Carney & Latham (1986).
- BD+06 0648: the temperature for this star is uncertain: the value we derive from colours and reddening by ATT is about 350 K lower than used in the analysis by Pilachowski et al. (1993, 1996) and Shetrone (1996). Use of a lower temperature would result in abundances in better agreement with the star's luminosity

8. Conclusions

We have determined Li, C, N, O, Na and Fe abundances, as well as ^{12}C/^{13}C isotopic ratios for a sample of 62 metal poor stars, originally selected to have -2 <[Fe/H]< -1, and accurate luminosities either from Hipparcos parallaxes or Anthony-Twarog & Twarog (1994). Statistically representative samples of 10-15 stars in each of the following evolutionary phases: main sequence and turn-off region, lower-RGB, upper-RGB, and RHB stars, were obtained. This already quite large sample has been then extended by considering literature data for Li, C, O, and Na, carefully reduced to the abundance system defined in the present paper. On the whole, we were able to derive abundances for 105 stars, more than two thirds of them with measured metallicities in the range -2 <[Fe/H]< -1 on our scale. Data in this well defined metallicity bin (which excludes massive thin disk stars, and extremely metal-poor stars for which original element-to-element abundance ratios may change by large factors) have been used to discuss mixing episodes along the red giant branch.

Our large set of uniform abundances shows that:

- There are two distinct mixing/dilution episodes along the RGB evolution of small mass, field stars. (i) The first dredge-up follows canonical predictions (see e.g. Charbonnel 1994,

1995). This is quite clear in the pattern shown by elements and isotopic ratios. The luminosity at which the first dredge-up occurs for this metallicity bin is about $\log L/L_{\odot} = 0.8$; Li is diluted by about a factor of 20, ^{12}C abundance decreases by about 0.05 dex. Any possible decrease in ^{12}C/^{13}C is not large enough to make ^{13}CH lines detectable. (ii) A second mixing episode occurs when the star becomes brighter than the RGB bump (and the molecular weight barrier is canceled) at $\log L/L_{\odot} \sim 2$ for the metallicity bin here considered, again in agreement with predictions by Charbonnel (1994, 1995). Most of the remaining Li is destroyed, the ^{12}C abundance further decreases by a factor of ~ 2.5, the ^{12}C/^{13}C ratio reaches a value of $\sim 6-10$, and the N abundance raises by nearly a factor of four. As expected from pure mixing of regions of CN-burning, the sum of C+N abundances remains constant. These values are observed also in the following evolutionary phases (RHB and early AGB).

– Mixing is apparently a function of metallicity, reaching a maximum value for [Fe/H]~ -1.5. At metallicities below [Fe/H]≤ -1.9 on our scale, a large scatter in [C/Fe] is observed for stars evolved off the RGB bump. However, it is not clear if this larger scatter is due to a scatter in the original element-to-element abundances (as observed for several elements by McWilliam et al. 1995), or rather to some factor modulating mixing efficiency
– O and Na abundances in upper-RGB and HB field stars are similar to those observed in unevolved stars. This confirms earlier results obtained for field RR Lyrae variables (Clementini et al. 1995). Field stars do not display any signature of the Na-O anticorrelation commonly seen amongst globular cluster giants (Kraft 1994), confirming on our more extended sample earlier results by Kraft et al. (1982), Kraft (1994), Pilachowski et al. (1996), and Shetrone (1996). We then propose that the presence of this Na-O anticorrelation is related to some significant difference between field and cluster stars, perhaps due to more dense environment in which cluster stars form and/or evolve.

Acknowledgements. We thank I. Ivans, B. Kraft, and C. Charbonnel for helpful and stimulating conversations. We thank C.R. James for obtaining some of the McDonald spectra. C.S. wishes to acknowledge Italian C.N.R. for financial support and Padova Observatory for its hospitality during his stay while the data were being analysed. R.G.G. thanks the John W. Cox Endowment for financial support for his visit to The University of Texas at Austin while this paper was being written. This research was supported by NSF grant AST 96-18364 to CS.

References

Alonso A., Arribas S., Martinez-Roger C., 1996, A&AS 117, 227
Anders E., Grevesse N., 1989, Geochim. Cosmochim. Acta 53, 197
Andersen J., Gustafsson B., Lambert D.L., 1984, A&A 136, 65
Anthony-Twarog B.J., Twarog B.A., 1994, AJ 107, 1577 (ATT)
Aoki W., Tsuji T., 1997, A&A 328, 175
Barbuy B., 1988, A&A 191, 121
Bard A., Kock M., 1994, A&A 282, 1014
Bard A., Kock A., Kock M., 1991, A&A 248, 315
Bell R.A., Eriksonn K., Gustafsson B., Nordlund A., 1976, A&A 23, 37
Beveridge C.R., Sneden C., 1994, AJ 108, 285
Biemont E., Hibbert A., Godefroid M., Vaeck N., Fawcett B.C., 1991a, ApJ 375, 818
Biemont E., Baudoux M., Kurucz R.L., Ansbacher W., Pinnington E.H., 1991b, A&A 249, 539
Blackwell D.E., Lynas-Gray A.E., Smith G., 1995, A&A 296, 217
Boesgaard A.M., King J.R., Deliyannis C.P., Vogt S.S., 1999, AJ 117, 492
Bond H.E., 1980, ApJS 44, 517
Bonifacio P., Molaro P., 1997, MNRAS 285, 847
Briley M.M., Bell R.A., Hoban S., Dickens R.J., 1990, ApJ 359, 307
Burstein D., Heiles C., 1982, AJ 87, 1165
Carbon D.E., Romanishin W., Langer G.E., et al., 1982, ApJS 49, 207
Carbon D.F., Barbuy B., Kraft R.P., Friel E.D., Suntzeff N.B., 1987, PASP 99, 335
Carney B.W., Latham D.W., 1986, AJ 92, 60
Carney B.W., Latham D.W., Laird J.B., Aguilar L.A., 1994, AJ 107, 2240
Carretta E., Gratton R.G., 1997, A&AS 121, 95
Carretta E., Gratton R.G., Sneden C., 1999, submitted to A&A
Cassisi S., Degl'Innocenti S., Salaris M., 1997, MNRAS 290, 515
Castelli F., Gratton R.G., Kurucz R.L., 1997, A&A 318, 841
Cavallo R.M., Pilachowski C.A., Rebolo R., 1997, PASP 109, 226
Charbonnel C., 1994, A&A 282, 811
Charbonnel C., 1995, ApJ 453, L41
Clementini G., Carretta E., Gratton R.G., et al., 1995, AJ 110, 2319
Clementini G., Gratton R.G., Carretta E., Sneden C., 1998, MNRAS 302, 22
Cottrell P.L., Sneden C., 1986, A&A 161, 314
Edvardsson B., Andersen J., Gustafsson B., et al., 1993, A&A 275, 101
Fuhrmann K., 1998, A&A 338, 161
Gratton R.G., 1988, Rome Observatory Preprint no. 29
Gratton R.G., 1989, A&A 208, 171
Gratton R.G., D'Antona F., 1989, A&A 215, 66
Gratton R.G., Ortolani S., 1986, A&A 169, 201
Gratton R.G., Ortolani S., 1989, A&A 211,41
Gratton R.G., Sneden C., 1991, A&A 241, 501
Gratton R.G., Gustafsson B., Carretta E., Eriksson K., 1999, A&A, in press
Gratton R.G., Carretta E., Matteucci F., Sneden C., 1996, In: Morrison H., Sarajedini A. (eds.) The Formation of the Galactic Halo... Inside and Out. ASP Conf. Ser. 92, p. 307
Grevesse N., Lambert D.L., Sauval A.J., et al., 1991, A&A 242, 488
Hannaford P., Lowe R.M., Grevesse N., Noels A., 1992, A&A 259, 301
Hanson R.B., Sneden C., Kraft R.P., Fulbright J., 1998, AJ 116, 1286
Harmer D.L., Pagel B.E.J., 1973, MNRAS 165, 91
Holweger H., Heise C., Kock M., 1990, A&A 232, 510
Iben I.Jr., 1964, ApJ 140, 1631
Iben I.Jr., Renzini A., 1984, Phys. Letters 105, 329
Israelian G., García Lopez R.J., Rebolo R., 1998, ApJ 507, 805
Jehin E., Magain P., Neuforge C., et al., 1999, A&A 341, 241
King C.R., Da Costa G.S., Demarque P., 1985, ApJ 299, 674
King J.R., 1997, AJ 113, 2302
King J.R., Deliyannis C.P., Boesgaard A.M., 1996, AJ 112, 2839
Kiselman D., 1991, A&A 245, 9
Kraft R.P., 1994, PASP 106, 553
Kraft R.P., Suntzeff N.B., Langer G.E., et al., 1982, PASP 94, 55
Kraft R.P., Sneden C., Langer G.E., Prosser C.F., 1992, AJ 104, 645
Kraft R.P., Sneden C., Smith G.H., et al., 1997, AJ 113, 279

Kurucz R.L., 1995, CD-ROM 13
Kurucz R.L., Furenlid I., Brault J., 1984, National Solar Observatory Atlas. National Solar Observatory, Sunspot, New Mexico
Laird J.B., 1985, ApJ 289, 556
Lambert D.L., 1978, MNRAS 182, 249
Lambert D.L., Luck R.E., 1978, MNRAS 183, 79
Lambert D.L., Sneden C., 1977, ApJ 215, 597
Langer G.E., Kraft R.P., 1984, PASP 96, 339
McWilliam A., Preston G.W., Sneden C., Searle L., 1995, AJ 109, 2757
Moore C.E., Minnaert M.G.J., Houtgast J., 1966, NBS Monog. no. 145
Nissen P.E., Schuster W.J., 1997, A&A 326, 751
Norris J.E., Ryan S.G., Beers T.C., 1997, ApJ 489, L169
Para A., 1991, At. Mol. Opt. Phys. 24, 3179
Pilachowski C.A., Sneden C., Booth J., 1993, ApJ 407, 699
Pilachowski C.A., Sneden C., Kraft R.P., 1996, AJ 111, 1689
Rossi S., Beers T.C., Sneden C., 1999, in preparation
Rutten R.J., Van der Zalm E.B.J., 1984, A&AS 55, 143
Schuster W.J., Nissen P.E., 1989, A&A 222, 69
Shetrone M.D., 1996, AJ 112, 1517
Shetrone M.D., Sneden C., Pilachowski C.A., 1993, PASP 105, 337
Sneden C., Pilachowski C.A., VandenBerg D.A., 1986, ApJ 311, 826
Sneden C., Kraft R.P., Prosser C.F., Langer G.E., 1991, AJ 102, 2001
Spite F., Spite M., 1982, A&A 115, 357
Spite M., Spite F., 1991, A&A 252, 689
Sweigart A.V., Mengel J.G., 1979, ApJ 229, 624
Tomkin J., Lemke M., Lambert D.L., Sneden C., 1992, AJ 104, 1568
Trefzger C.F., Langer G.E., Carbon D.E., Suntzeff N.B., Kraft R.P., 1983, ApJ 266, 144
Tull R.G., McQueen P., Sneden C., Lambert D.L., 1995, PASP 107, 251
VandenBerg D.A., Smith G.H., 1988, PASP 100, 314
Westin J., Sneden C., Gustafsson B., Cowan J.J., 1999, ApJ in press
Wilson O.C., 1962, ApJ 136, 793
Zhao G., Magain P., 1990, A&AS 86, 85
Zoccali M., Cassisi S., Piotto G., Bono G., Salaris M., 1999, ApJ 518, L49